A computational study of the interaction of gaseous detonations with a compressible layer

Maxime Reynaud, Florent Virot, Ashwin Chinnayya

A Computational Study of the Interaction of Gaseous Detonations with a Compressible Layer

Maxime Reynaud,[1, a)] Florent Virot,[1, b)] and Ashwin Chinnayya[1, c)]

[1] *Institut* Pprime, *UPR 3346 CNRS, ISAE – ENSMA and University of Poitiers, BP 40109, 86961 Futuroscope-Chasseneuil cedex, France*

(Dated: May 17, 2017)

The propagation of two-dimensional cellular gaseous detonation bounded by an inert layer is examined via computational simulations. The analysis is based on the high-order integration of the reactive Euler equations with a one-step irreversible reaction. To assess whether the cellular instabilities have a significant influence on a detonation yielding confinement, we achieved numerical simulations for several mixtures from very stable to mildly unstable. The cell regularity was controlled through the value of the activation energy, while keeping constant the ideal Zel'dovich - von Neumann - Döring (ZND) half-reaction length. For stable detonations, the detonation velocity deficit and structure are in accordance with the generalized ZND model, which incorporates the losses due to the front curvature. The deviation with this laminar solution is clear as the activation energy is more significant, increasing the flow field complexity, the variations of the detonation velocity and the transverse wave strength. The chemical length scale gets thicker, as well as the hydrodynamic thickness. The sonic location is delayed due to the presence of hydrodynamic fluctuations, of which the intensity increased with the activation energy as well as with the losses to a lesser extent. The flow field has been studied through numerical soot foils, detonation velocities and 2D detonation front profiles, which are consistent with experimental findings. The velocity deficit increases with the cell irregularity. Moreover, the relation between the detonation limits obtained numerically and in detonation experiments with losses is discussed.

[a)] maxime.reynaud@ensma.fr

[b)] florent.virot@ensma.fr

[c)] Corresponding author: ashwin@ensma.fr

I. INTRODUCTION

A gaseous detonation consists of an exothermic chemical reaction coupled to a supersonic shock wave that propagates through a detonable medium. The very rapid energy conversion leads to consider the detonation as an alternative to the more classical combustion in the aeronautical engines. However, many issues arise from its potential use for propulsion applications[1]. As for the rotating detonation engine, the combustion chamber is usually an annular ring composed of the walls of two coaxial cylinders. Subsequently to the injection at the bottom-end, detonation fronts propagate circumferentially into the fresh mixture. The expansion of the detonation products through the engine top-end creates a continuous thrust. Prior to the arrival of the detonation, the burned gases generated by the previous front confine the freshly injected reactive material. Thus, the flow field within the combustion chamber highlights a complex shock/detonation structure and, most of the time, a deficit of the detonation velocity[2,3]. A better understanding of the underlying physical phenomena is needed in order to ensure the design of this new propulsion device[4,5].

The velocity at which a detonation is propagating through the reactive material is an essential data. The simple theory developed by Chapman and Jouguet (CJ) at the beginning of the latter century states that the steady detonation velocity is the minimum velocity compatible with the conservation laws[6]. This model provides very accurate results in predicting the detonation velocity in the knowledge that only the initial state and thermodynamic properties were required to perform the calculations. Moreover, no assumption on the kinetics mechanism is needed as the products are in thermochemical equilibrium and the reaction is considered to occur instantaneously. Consequently, the influence of boundary conditions such as walls or confinements cannot be taken into account. For this reason, models have to include a reaction zone of finite thickness. In his initial work, Zel'dovitch[7] attempted to incorporate the effects of heat and momentum losses into the Zeldovich - von Neumann - Döring (ZND) model. However, the wall forces distribution was incorrectly represented and led to inaccurate results. Fay[8] focused on the influence of the boundary layer which develops in tubes downstream of the leading shock. He treated the induced negative displacement layer as a flow divergence, leading to a curved detonation. The friction induced by the walls are thus analogous to the effects produced by the lateral expansion of the detonation products towards the yielding confinement. This is responsible for the front curvature[9]. See the

monograph from Lee[10] for a review on the effect of boundary conditions on the detonation dynamics.

The very early steady models for 2D detonations were proposed by Jones[11] and Eyring et al.[12] They established a relationship between the detonation velocity in cylindrical explosives and the radius of the charge. Wood and Kirkwood[13] (WK) developed a quasi-1D model by restraining the analysis of the two-dimensional Euler equations on the central streamline. Assuming that the radius of curvature is large relatively to the reaction-zone thickness, they put forward a link between the velocity deficit of the detonation and the shock front curvature. Bdzil[14] generalized the WK model in two dimensions. He supposed that the streamline deflection angle remains small, which can be justified in the case of high-density explosives.

The first experiments on gaseous detonation confined by a compressible layer were performed by Sommers[15], Sommers and Morrison[16], Dabora[17] and Dabora et al[18]. They aimed to study the influence of the condensed explosives confinement by analogy with the propagation of a gaseous detonation bounded by an inert gas layer. The resulting Schlieren photographs showed the main features of this configuration: the front curvature, the attached oblique shock wave and the interface between burned gases and inert gases. Similar experiments were also performed by Adams[19,20], Murray and Lee[21] and Vasil'ev and Zak[22]. In the context of hydrogen safety, a recent resurgence of interest in the weak confinement of detonations led to the development of new experiments. Rudy et al.[23–25] and Grune et al.[26] investigated the critical layer thickness enabling the propagation of detonations in a partially confined channel, and corroborated the values obtained by Dabora et al.[18]

Oran and Gamezo[27] achieved numerical simulations of detonations bounded by an inert medium, confirming Bdzil's findings[14]. More recently, Li et al.[28] performed computational simulations in two different geometries (cylindrical tube and two-dimensional slab) and made meaningful comparisons of the detonation curvature with ad hoc models. The latter authors also investigated the influence of confinement with various acoustic impedance ratios. They concluded that the model based on Eyring[12] and Wood and Kirkwood[13] theories achieved a remarkably good evaluation of the detonation velocity as a function of the curvature of the leading front. However, the reaction rate used in the aforementioned paper is only pressure-dependent, thus preventing the development of cellular instabilities. In another study Li et al.[29] studied the influence of spatial heterogeneities on the propagation limits of

a bounded detonation. Sinusoidal ripples of density were created upstream of the laminar detonation wave and were shown to enhance the resistance to failure. However, the nature of the heterogeneities prevents from building generalized conclusions about the behaviour of gaseous cellular detonations. Thus, the behavior of detonations yielding confinement and the accuracy of the models as far as intrinsic instabilities are concerned, remains an issue.

Experimental and numerical researches in the last sixty years have both attested to the unsteady and three-dimensional nature of gaseous detonations[10]. Two-dimensional detonation fronts, as they can be observed in rectangular tubes with a large aspect ratio, consist of an alternation of strong Mach stems and weaker incident shocks. They intersect with the transverse waves at the triple points, whose the trajectories form the cellular structure of the detonation. This cellular pattern of varying degree of regularity may be classified from excellent to irregular[30,31] as a function of the initial pressure and the level of dilution of the fresh gases.

In order to form a better view on the role played by transverse waves interaction on the propagation of irregular detonations, Radulescu and Lee[32] performed well-diagnosed experiments in porous walls and investigated whether the failure was caused by the damping of the transverse waves rather than the flow leaking into the porous walls. They concluded that the ignition by the leading shock was responsible of the propagation of stable detonations in argon-diluted mixtures. In highly unstable mixtures characterized by very irregular cellular patterns, the propagation mechanism was noticeably different and closely linked to the ability of generating a sufficient number of transverse waves to counterbalance the losses.

To assess whether those instabilities have a significant influence on a detonation yielding confinement, we achieved numerical simulations of detonations bounded by an inert gas layer for several mixtures from very stable to mildly unstable. The regularity of the mixture was directly controlled through the value of the activation energy, while the length scale of the ideal ZND model was kept constant. The flow field structure was analyzed through the investigation of numerical soot foil plates. Furthermore, we evaluated the dependency between the detonation frontal curvature and its velocity deficit, and we compared the results with those obtained from a model based on the WK theory. This paper addresses the role of the cellular structure on the detonation propagation and failure, as losses are due to the weak confinement and also to the fluctuations which develop through the subsonic reaction zone and which can act as an energy withdrawal. The governing equations are

presented in §2. Section 3 describes the numerical solver employed, presents the physical configuration and the analytical model used. Section 4 presents the numerical simulations and their analysis. Finally, we conclude this paper in §5 with further discussions on the results obtained throughout this study.

II. GOVERNING EQUATIONS

In this study, the flow is regarded as a compressible reactive ideal gas governed by the two-dimensional system of Euler equations:

$$\frac{\partial U}{\partial t} + \frac{\partial F(U)}{\partial x} + \frac{\partial G(U)}{\partial y} = S(U) \tag{1}$$

The conserved variable vector U, the directional convective flux vectors F and G and the chemical source term vector S are given by

$$U = \begin{bmatrix} \rho \\ \rho u \\ \rho v \\ \rho E \\ \rho Y \end{bmatrix}, F = \begin{bmatrix} \rho u \\ \rho u^2 + p \\ \rho uv \\ (\rho E + p)u \\ \rho Y u \end{bmatrix}, G = \begin{bmatrix} \rho v \\ \rho uv \\ \rho v^2 + p \\ (\rho E + p)v \\ \rho Y v \end{bmatrix}, S = \begin{bmatrix} 0 \\ 0 \\ 0 \\ 0 \\ -\rho\dot{\omega} \end{bmatrix}$$

Here, ρ, p, u, v and Y are the density, the pressure, the velocities and the reaction progress variable, respectively. $Y = 1$ when the gases are completely burned. Assuming a calorically perfect ideal gas, the total energy E is expressed as

$$E = e + \frac{u^2 + v^2}{2} - Yq, \text{ with } e = \frac{p}{(\gamma - 1)\rho} \tag{2}$$

q is the heat release and γ is the ratio of specific heats. A one-step global irreversible reaction of the form $\mathcal{R} \rightarrow \mathcal{P}$ is used to model the chemical process by which the reactants are transformed into the products. The chemical source term follows the standard Arrhenius law,

$$\dot{\omega} = k(1 - Y)\exp\left(\frac{-E_a}{RT}\right) \tag{3}$$

where k, E_a and R are the pre-exponential factor, the activation energy and the gas constant, respectively. The reaction was artificially inhibited when the mass fraction reaches the value

of $\epsilon = 10^{-3}$ in order to ensure that the reaction length remained finite. Additionally, a pressure threshold was implemented so as to prevent the reaction to occur prior to the leading shock. Single-step chemistry is widely used to simulate detonations and exhibits a good agreement with the experiments[33]. Even characteristic features of very unstable mixtures, such as methane – air, are correctly retrieved[34]. However, several effects such as the double cellular detonation structure cannot be described by this model[35]. These effects are not present in the present study, as the highest action energy corresponds to a mildly unstable mixture. Moreover, the implementation of a detailed chemical kinetics does not give more accurate results than reduced models. Taylor et al.[36]argue that thermodynamic non-equilibrium has to be taken into account for the mixtures at atmospheric pressure. The aim of this work is to highlight the flow features of the detonation confined by an inert layer.

Four different values of the reduced activation energy E_a/RT_0 were employed in this study to control the detonation stability: 10, 20, 30 and 38.23. The last one corresponds to a single-step mechanism calibrated using data for detonations of a stoichiometric hydrogen/oxygen mixture at the initial pressure of 1 atm and at the initial temperature of 295 K. The three others model a fictive mixture of lower sensitivity with the same thermodynamic parameters. These thermodynamic parameters were chosen to be approximately those of a stoichiometric hydrogen/oxygen mixture at the initial pressure of 1 atm and the initial temperature of 295 K. The ratio of specific heats and the heat release are given by $\gamma = 1.333$ and $q = 4.867$ MJ/kg, i.e. $q/RT_0 = 23.81$, respectively[37,38]. Corresponding CJ and von Neumann (vN) parameters are $D_{\mathrm{CJ}} = 2845$ m/s, $P_{\mathrm{CJ}} = 17.5$ bar, $T_{\mathrm{CJ}} = 3007$ K, $P_{\mathrm{vN}} = 34.0$ bar and $T_{\mathrm{vN}} = 1707$ K. The Mach number is then $M_{\mathrm{CJ}} = 5.53$. The numerical simulations presented in §4 were performed for different values of the reduced activation energy E_a/RT_0. For each value of E_a/RT_0, the pre-exponential factor of the Arrhenius law was adjusted so as to keep the half-reaction length $l_{1/2}$ constant. The half-reaction length is defined as the distance between the incident shock and the position where $Y = 1/2$ in the ideal ZND model without losses. This led to a cell size roughly constant for the different activation energies, which greatly facilitates the flow field analysis. Thus, the calibrations were made so that the simulated cell size of a detonation without losses propagating in a wide channel was typical of a stoichiometric hydrogen/oxygen mixture in those conditions of pressure and temperature, *i.e.* $E_a/RT_0 = 38.23$ and $\lambda \approx 2$ mm[39]. The half-reaction length obtained for these parameters via an ideal ZND calculation is $l_{1/2} = 90.79$ µm.

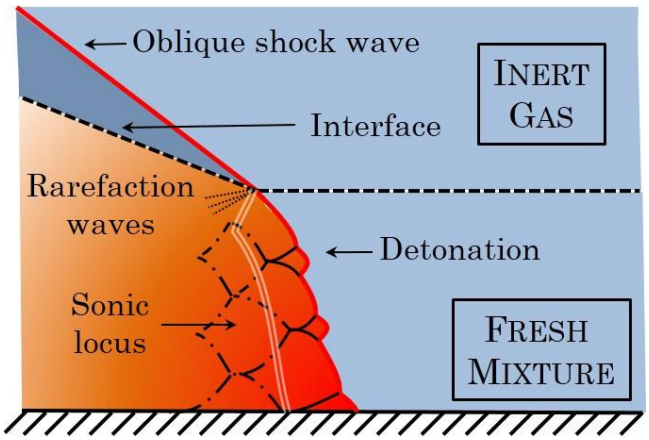

Figure 1: Schematic of the numerical configuration. A detonation wave propagates from the left to the right into a reactive medium bounded by an inert gas.

III. NUMERICAL METHOD

A. Numerical solver

In this work, we employed a classical time-operator splitting method in order to couple the hydrodynamics to the chemistry and to accommodate the stiffness due to the wide range of time scales. A directional splitting is also used. The characteristic variables were reconstructed on the cell boundaries using a ninth-order Monotonicity Preserving interpolation[40]. High-order numerical schemes are advocated, since they lead to a reduced dissipation and a better accuracy, even in the presence of strong shocks[41,42].The fluxes through the interfaces were computed by solving the Riemann problem by means of the approximate Harten - Lax - van Leer (HLLC) solver"[43]. The temporal-integration was accomplished using a third-order Total Variation Diminishing (TVD) explicit Runge-Kutta method. The parallelization of the code was achieved through a domain decomposition method. The communications between the different processors were held by the Messaging Passing Interface (MPI) standard. The largest simulations were performed on 400 processors with a typical cost of $\sim$ 60,000 CPU scalar hours.

B. Problem statement

The physical configuration associated with the numerical simulations is depicted on the Figure 1. The detonation travels from left to right in the positive x direction and propagates into a medium at rest composed of a gaseous reactive layer bounded by an inert gas. Slip boundary conditions were used on the lower wall and outflow conditions were employed on the other boundaries. At time $t = 0$, the domain was entirely filled with fresh reactive mixture. The detonation was initiated by setting an area at the von Neumann state. This region was located in the middle of the domain in the x direction and was as high as the reactive layer. Then, the flow gradually evolved from the initial vN-region to an overdriven combined wave and ultimately reached a quasi-steady propagation state independent from the ignition and the initial conditions. The front curvature increased progressively as the high-pressure products expanded toward the upper compressible layer. Kelvin-Helmholtz instabilities appeared on the interface between the burned gases and the inert gas. The oblique shock leaned over in the inert gas until it reached its final slope. Depending on the reactive layer height, transverse instabilities arose and gave birth to the cellular structure of the detonation.

A specific recycling procedure has been implemented to limit the calculation length. During the course of the simulation when the leading shock reached the right boundary of the computational domain, a new region was appended to the right of the computational domain and another was discarded on the opposite side. As the removal occurred beyond the characteristic line delimiting the sonic locus in the steady case, this process does not have any influence on the detonation propagation[44]. In front of the detonation wave, the new area was implemented with the upstream conditions: the lower layer was filled with fresh mixture and the upper layer with an inert gas. This process arose periodically during the computation of the detonation propagation and enabled the calculation to be performed on smaller computational domains, thus allowing a higher numerical resolution. This recycling process has been successfully used to simulate the propagation of detonations by Sow[45] and Li et al[28,29]. Further, the detonation front mainly evolves in a restricted area close to the right boundary. Consequently, a static mesh refinement method based on the MPI topology was implemented, as illustrated in Fig. 2. Finer meshes were used at the vicinity of the detonation front whereas the spatial resolution decreased by a factor of two as the

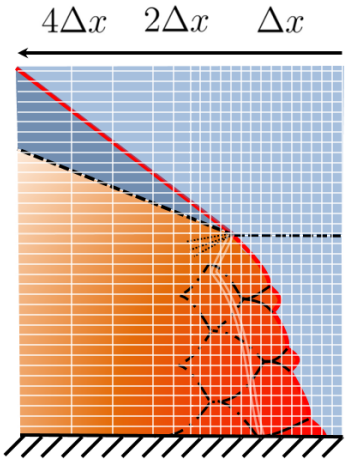

Figure 2: Schematic of the static mesh refinement method. In this example two levels of refinement are employed.

computational cells were more distant from the detonation wave. The numerical resolution in finest grid consisted of $N_{1/2} = 30$ points per half-reaction length except for the mixture with $E_a/RT_0 = 38.23$ where the size of the computational domain needs to be enlarged and thus prevents from using such a resolution. For this case, $N_{1/2}$ was lowered to ten points per half-reaction length. Although this resolution seems low for such mildly unstable detonations, the average quantities calculated in simulations with $N_{1/2} = 15$ and 20 agree well with each other. The mean pressure and the averaged local Mach number are plotted for different resolutions in the Figure 3. The conclusions of this study are thus not called into question relatively to this issue.

The overall size of the domain was chosen according to the reactive layer height h, which depends on the activation energy. The simulations reveal that as E_a/RT_0 increased, the critical height allowing the self-sustained propagation of the combined wave increased as well. As a consequence, the number of computational cells N also augmented. This trend will be addressed in the next Section. As far as the cellular structure of the detonation (*i.e.* 2D instabilities) is concerned, we observed the development of transverse waves in most cases. For the simulations computed with $E_a/RT_0 = 10$ and $E_a/RT_0 = 20$, detonation cells began to appear starting from $h = 5.0$ mm. For higher values of the reduced activation energy, i.e. $E_a/RT_0 = 30$ and 38.23, the cellular structure was present regardless of the reactive layer height. The cell size λ for each activation energy was measured on numerical soot plates by averaging the value on more than 50 detonation cells. The parameters used

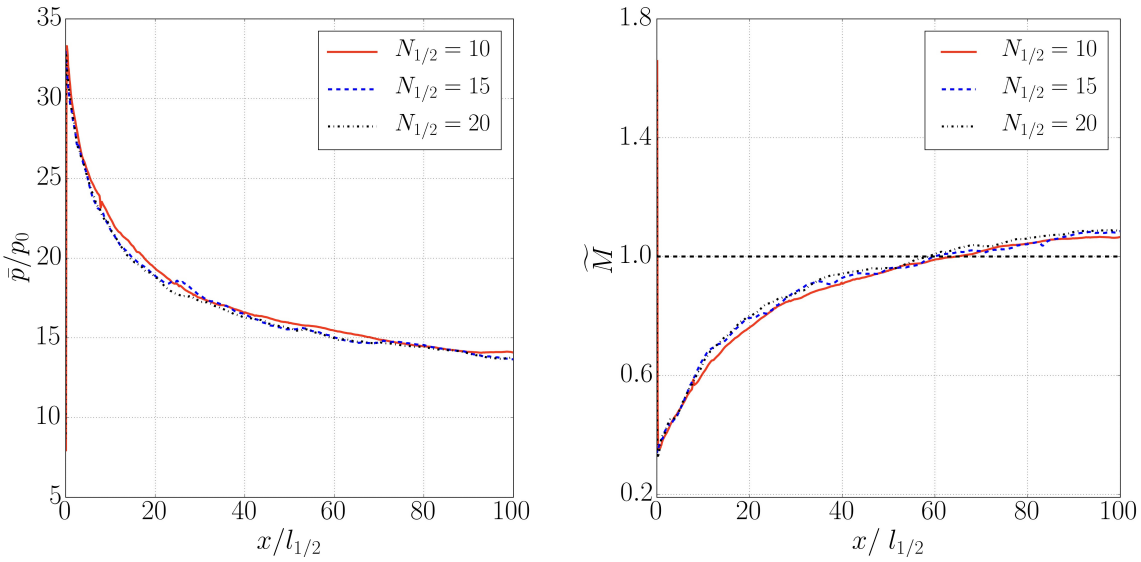

(a) (b)

Figure 3: Influence of the numerical resolution on the average pressure normalized by p_0 (a) and on the mean local Mach number (b) for a mixture with $E_a/RT_0 = 38.23$ and $h = 45$ mm $= 496\ l_{1/2}$.

E_a/RT_0	E_a/RT_{vN}	$l_{1/2}$ (µm)	$N_{1/2}$	N ($\times 10^6$)	λ (mm)	$k_{1/2} = \lambda/l_{1/2}$
10	1.73	90.79	30	2.0 - 4.2	1.3	14
20	3.46	90.79	30	2.5 - 4.2	1.7	19
30	5.18	90.79	30	30 - 45	2.1	23
38.23	6.61	90.79	10	27	1.9	21

Table I: Summary of the numerical parameters. $l_{1/2}$ is the half-reaction zone, $N_{1/2}$ the number of points per $l_{1/2}$, N the total number of cells, λ the cell size in the ideal case and $k_{1/2}$ the ratio of the cell size in the ideal case to the half-reaction length.

in our calculations are summarized in the Table I. The length of the domain was chosen to incorporate the sonic line and was also function of the domain height because of the front curvature. These constraints led to a computational domain that was 3 times the cell size long and 5 times the cell size high for the lowest activation energy. For the highest activation energy, the domain was 20 times the cell sizes long and 30 times the cell size high.

Numerical simulations have shown that one-dimensional detonations exhibit an unstable

behavior depending on the kinetics and thermodynamics properties of the mixture[46,47]. It has been demonstrated that for other parameters fixed, it exists a critical value of the activation energy beyond which the ideal ZND steady solution acquires a pulsating nature[48]. Then, with the increase of the activation energy, the instabilities evolve from a simple cyclic mode to a complex and chaotic character, following a period-doubling pattern[49]. For our thermodynamics parameters, one-dimensional simulations reveal that these instabilities are absent with the exception of $E_a/RT_0 = 38.23$ where these longitudinal oscillations are present.

C. Model

The flow divergence due to the inert layer can be incorporated into the one-dimensional ZND model. Following the approach of Wood and Kirkwood[13], the flow is assumed to be compressible, non-dissipative, adiabatic and reactive. In addition, the detonation is supposed to propagate in a steady and laminar state. Thus, the Euler equations Eqs. 1 can be rewritten in the shock coordinates $\bar{u} = D - u$. The bar is omitted in the following equations for clarity.

$$\begin{cases} \dfrac{\partial \rho u}{\partial x} + \dfrac{\partial \rho v}{\partial y} = 0 \\ \dfrac{\partial (\rho u^2 + p)}{\partial x} + \dfrac{\partial \rho u v}{\partial y} = 0 \\ \dfrac{\partial \rho u v}{\partial x} + \dfrac{\partial (\rho v^2 + p)}{\partial y} = 0 \\ \dfrac{\partial (\rho E + p) u}{\partial x} + \dfrac{\partial (\rho E + p) v}{\partial y} = 0 \\ \dfrac{\partial \rho u Y}{\partial x} + \dfrac{\partial \rho v Y}{\partial y} = -\rho \dot{\omega} \end{cases} \tag{4}$$

The analysis is restrained to the bottom wall streamline $y = 0$, which implies that the spanwise velocity v is null. Consequently, the system of Eqs. 4 can be rewritten as follows in the shock coordinates:

$$\begin{cases} \dfrac{\mathrm{d}u}{\mathrm{d}x} = -\dfrac{(\gamma - 1) q \dot{\omega} - c^2 \omega_r}{c^2 - u^2} \\ \dfrac{\mathrm{d}\rho}{\mathrm{d}x} = -\dfrac{\rho}{u} \left(\dfrac{\mathrm{d}u}{\mathrm{d}x} + \omega_r \right) \\ \dfrac{\mathrm{d}p}{\mathrm{d}x} = -\rho u \dfrac{\mathrm{d}u}{\mathrm{d}x} \\ \dfrac{\mathrm{d}Y}{\mathrm{d}x} = -\dfrac{\dot{\omega}}{u} \end{cases} \tag{5}$$

$\omega_r = \dfrac{\partial v}{\partial y}(y=0)$ denotes the curvature term. The determination of the velocity divergence on the wall streamline can be determined via a geometrical analysis[6]:

$$\omega_r = \frac{D - u_{\mathrm{vN}}}{\mathcal{R}} \tag{6}$$

Through an asymptotic analysis, Klein and Stewart[50] showed that:

$$\omega_r = \frac{D - u(x)}{\mathcal{R}} \tag{7}$$

The latter closure term was preferred rather than Eq. 6 as it showed a better accuracy. Given the post-shock state as initial conditions, the Eqs. 5 can be integrated until the generalized CJ conditions are satisfied, i.e. until $\bar{u} = c$ (sonic condition) and $(\gamma-1)q\dot{\omega} = c^2\omega_r$ (thermicity condition). By repeating this process for several radius of curvature, we obtained the classical "backwards C" curve[51] which depicts the detonation velocity as a function of the losses encountered.

IV. RESULTS

A. Detonation velocity deficit

During each simulation, the averaged detonation velocity $\bar{D}$ and the averaged front curvature $\mathcal{R}$ were calculated. The position of the leading shock at the bottom wall was obtained from the detection of the first pressure change in the initial medium (0.1% of the initial value). After interpolation using the Savitzky-Golay algorithm[52], which consists in fitting successive subsets of adjacent data with a polynomial fit by a linear least square method, the derivative of the initial signal was then evaluated leading to the detonation velocity as a function of time, from which the average velocity $\bar{D}$ could be calculated. The interpolation used in the Savitzky-Golay algorithm uses a 10^{th} order polynomial on a stencil of 10 points.

The mean curvature of the detonation front was computed from the averaged shape of the combined wave. At each time step, the position of every point constituting the leading shock was also detected by means of a pressure threshold and then averaged during the simulation by the following discrete mean procedure[53]. Consider the temporal mean $\bar{\psi}$ of a given variable ψ

$$\bar{\psi} = \lim_{\mathcal{T}\to\infty} \frac{1}{\mathcal{T}} \int_{t^0}^{t} \psi \mathrm{d}t \tag{8}$$

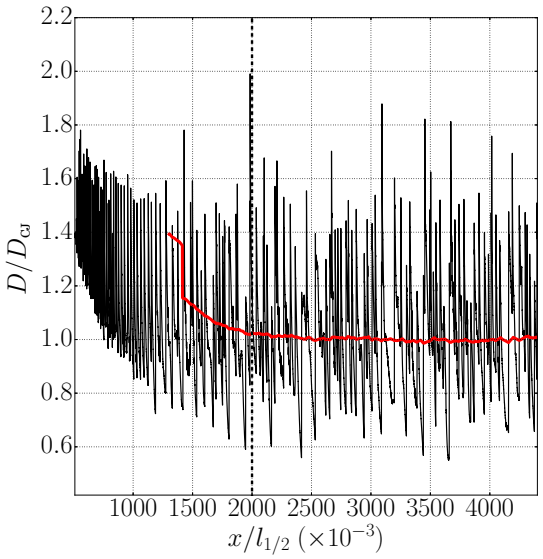

Figure 4: Instantaneous velocity of the detonation front normalized by D_{CJ} as a function of the distance elapsed from the initial pressure burst (black line) and average velocity (red line) with $E_a/RT_0 = 30$ and $h = 17$ mm.

where $\mathcal{T} = t - t^0$ is the sampling period. First-order integration gives

$$\bar{\psi} = \lim_{n\to\infty} \bar{\psi}^n \text{ with } \bar{\psi}^n = \frac{1}{t^n - t^0} \sum_{i=n_0}^{n} \psi^i (t^{i+1} - t^i) \tag{9}$$

This can be expressed as a numerical sequence

$$\bar{\psi}^{n+1} = \bar{\psi}^n - \frac{\Delta t^{n+1}}{t^{n+1} - t^0} (\bar{\psi}^n - \psi^{n+1}) \tag{10}$$

The value of t^0 was set at the end of the calculation initialization to ensure that the results remain independent of initial conditions. The mean position of the shock-detonation combined wave was then symmetrically extended beyond the horizontal axis and a fourth-order polynomial was fitted with the detonation front. The knowledge of the polynomial equation thus led to the mean curvature $\mathcal{R}$ at the bottom wall.

Prior to the averaging process, we ensure that the detonation has travelled about 2,000 $l_{1/2}$ ($\simeq 20\lambda$), ensuring independence from initial conditions. This criterion is based on the instantaneous velocity of the detonation as a function of the distance elapsed from the initial high-pressure burst. During the first transient phase of the simulation, the detonation is clearly overdriven as a result of this initiation process (see Fig. 4). The quasi-static state of propagation is then reached between 1,000 and 2,000 half-reaction lengths. The evolution

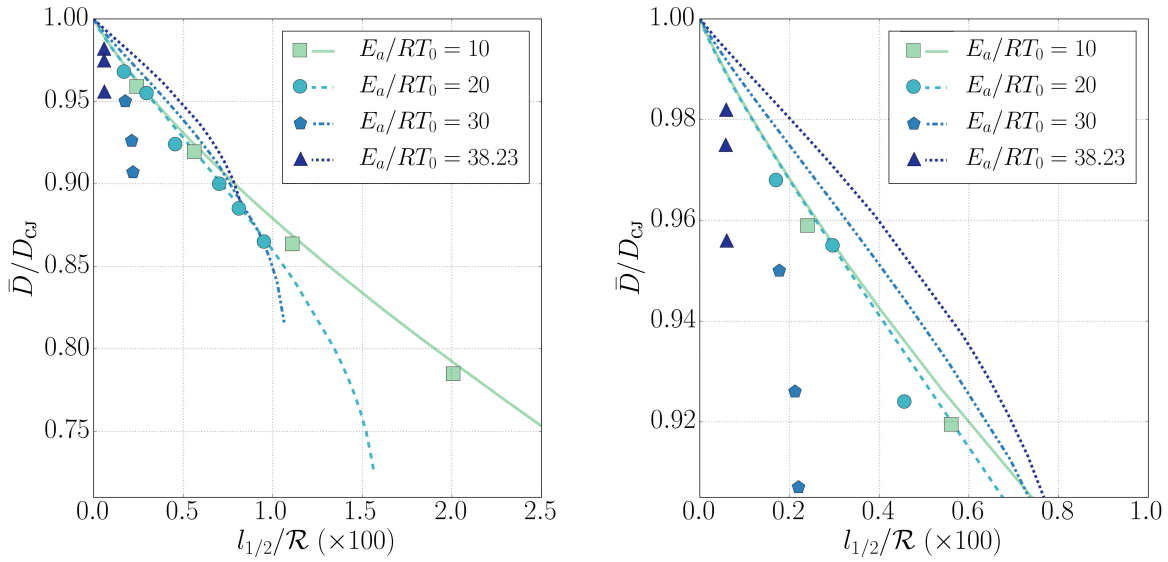

(a) (b)

Figure 5: Mean velocity deficit of the detonation front as a function of the averaged radius of curvature normalized by the half-reaction length from the numerical simulations (symbols) and comparison with the results from the WK model (lines). The Figure (b) is an enlargement of the Figure (a)

.

of the mean detonation velocity is depicted by the red curve and it has been estimated with running average with a sample of 30,000 points, approximately 970 half-reaction lengths. It should be also remarked that 2,000 half-reaction length is the propagation length necessary to ensure independence from the initial conditions, but that much more distance has to be travelled in order to build the averages profiles on the wall ($y = 0$).

The detonation velocity dependence on the front curvature as obtained from both the WK model and the bidimensional simulations are shown in the Figure 5. The velocity deficits $\bar{D}/D_{\mathrm{CJ}}$ are plotted as a function of $l_{1/2}/\mathcal{R}$ for the different reduced activation energies E_a/RT_0. The lines depict the generalized ZND solutions obtained by the WK model and demarcate the theoretically existence domain of stable detonations subject to losses. The velocity deficit of the detonation front increases proportionally to the averaged curvature until a turning point is reached beyond which the WK model does not provide any solution. This may be interpreted as a limit below which the velocity deficit cannot be endured by

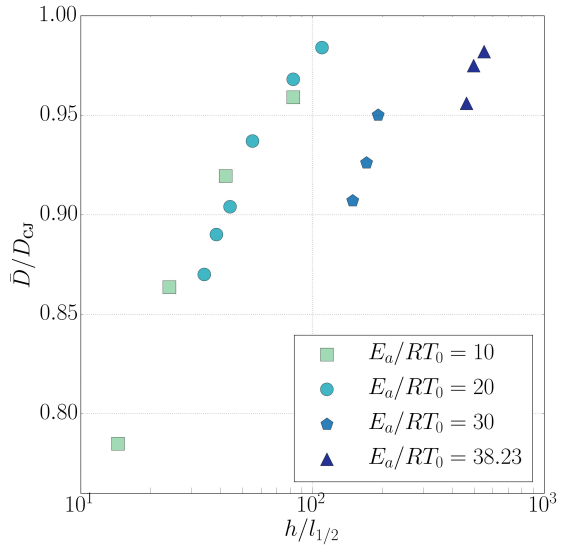

Figure 6: Mean velocity deficit of the detonation front as a function of the height of the reactive layer normalized by the half-reaction length, from the numerical simulations

.

the detonation anymore and thus leads to its quenching[54].

The symbols represent the results obtained as the outcome of the bidimensional simulations for the different values of E_a/RT_0. Each data set of the same color corresponds to a single value of the activation energy. By varying the height of the reactive layer upstream of the front, we influenced directly the losses encountered by the detonation and therefore its velocity deficit. Each distinct point relates to one simulation in which the reactive layer height is constant. The WK model appropriately retrieves the velocity deficit for $E_a/RT_0 = 10$ and $E_a/RT_0 = 20$. However, the points derived from the numerical simulations performed with $E_a/RT_0 = 30$ and $E_a/RT_0 = 38.23$ clearly follow a different trend. For the same radius of curvature, the velocity deficit obtained in the unsteady simulations is more important than predicted by the model. In the Figure 6, the velocity deficit of the detonation is plotted as a function of this height.

This discrepancy may be linked to the presence of one-dimensional longitudinal instabilities. One-dimensional calculations have demonstrated the absence of these instabilities for $E_a/RT_0 = 10, 20$ and 30. The threshold demarcating their appearance in the ideal case hence lies between $E_a/RT_0 = 30$ and $E_a/RT_0 = 38.23$. Nevertheless, Dionne et al.[55] have shown that the wall friction increases the effective activation energy and renders the detona-

tion more unstable. Later, Watt and Sharpe[56] reported that the neutral stability boundary of the detonation is lowered by the curvature effects. In other words, they argued that the detonation experiencing losses in its reaction zone may be unstable even if the corresponding planar detonation is stable in the one-dimensional sense. In our case, this means that the neutral stability boundary may be lower than $E_a/RT_0 = 30$, and thus that the one-dimensional instabilities can be at the root of the discrepancy between the numerical simulations and the WK model. These results are consistent with the numerical results of Sow et al.[57] who found that the velocity deficit due to both the presence of pulsating dynamics and 1D momentum and heat losses was under-predicted by the analytical model.

On the other hand, we reported the presence of transverse waves for simulations with $E_a/RT_0 = 10$ and 20 as well as for higher values of E_a/RT_0. Consequently, the differences between the WK model and the numerical results for activation energies higher than 30 cannot be uniquely and directly due to the existence or absence of the cellular structure. Rather, it may be related to the nature of the cellular structure. As it will be addressed in the next subsections, the transverse waves range from simple 'acoustic' perturbations to much stronger waves essential to the detonation propagation.

If the height of the reactive layer is smaller than a critical value h_{lim}, the detonation fails to reach its autonomous state of propagation, and quenches. This critical height depends on the reduced activation energy, as it can be observed in the Table II. As expected, the critical velocity deficit D_{lim} increases with the activation energy for both the WK model and the bi-dimensional results. In addition, regardless of the value of E_a/RT_0, the WK model under predicts the critical velocity deficit of the detonation compared to the values from the numerical simulations. The present results are in accordance with the recent numerical results of Borzou and Radulescu[58] on weakly unstable detonations, who have studied the behavior of detonations subject to a constant geometric mean flow divergence.

These initial results demonstrate the existence of two distinct behaviors. The first one corresponds to the physics described by the WK model and to the mixtures with a low activation energy. The second one is related to the more unstable mixtures for which the hypotheses of the steady model and laminar Eqs. 5 are unsatisfactory.

	$h_{\rm lim}/l_{1/2}$	$h_{\rm lim}/\lambda$	$D_{\rm lim}/D_{\rm CJ}$	$(D_{\rm lim}/D_{\rm CJ})_{\rm WK}$
$E_a/RT_0 = 10$	14.5	1.01	0.78	0.56
$E_a/RT_0 = 20$	34.1	1.82	0.86	0.74
$E_a/RT_0 = 30$	149	6.44	0.91	0.85
$E_a/RT_0 = 38.23$	462	20.0	0.96	0.88

Table II: Summary of the data about the limit of the detonation propagation obtained from the bi-dimensional simulations and the WK model.

B. Global features

This subsection is devoted to the study of the instantaneous features of the flow field in order to address the differences obtained previously between the different mixtures and shown in Section IV A.

1. $E_a/RT_0 = 20$

The two snapshots shown in the Figure 7 illustrate the propagation of the detonation-shock combined wave with a velocity deficit of 4%. The mixture is characterized by a reduced activation energy $E_a/RT_0 = 20$ and the reactive layer height is $h = 82.6\ l_{1/2}$. The detonation has travelled about 2,000 $l_{1/2}$ ($\simeq 20\lambda$), ensuring independence from initial conditions. During the first transients, the detonation is overdriven as a result of the initiation process, which consists of an high-pressure burst. The detonation then relaxes to the quasi-static state of propagation. The Figures 7(a) and 7(b) display the temperature field T normalized by T_0 and the mass fraction field Y, respectively. The Figure 7(a) allows the identification of the main features of the combined wave: the detonation front, the oblique shock wave and the interface between the burned gases and the inert gas. This picture also attests to the presence of transverse waves, moving back-and-forth in a transverse manner. Therefore, the detonation front presents irregularities due to the alternation between the Mach stems and the incident shocks. The velocity disparities between these two shocks lead to local variations of the curvature. The trajectory of the triple points as they move upward beyond the reactive layer is responsible for the saw-tooth shape of the interface between the burned gases and the inert gases. The triple point collisions produce two jets of hot gases oriented

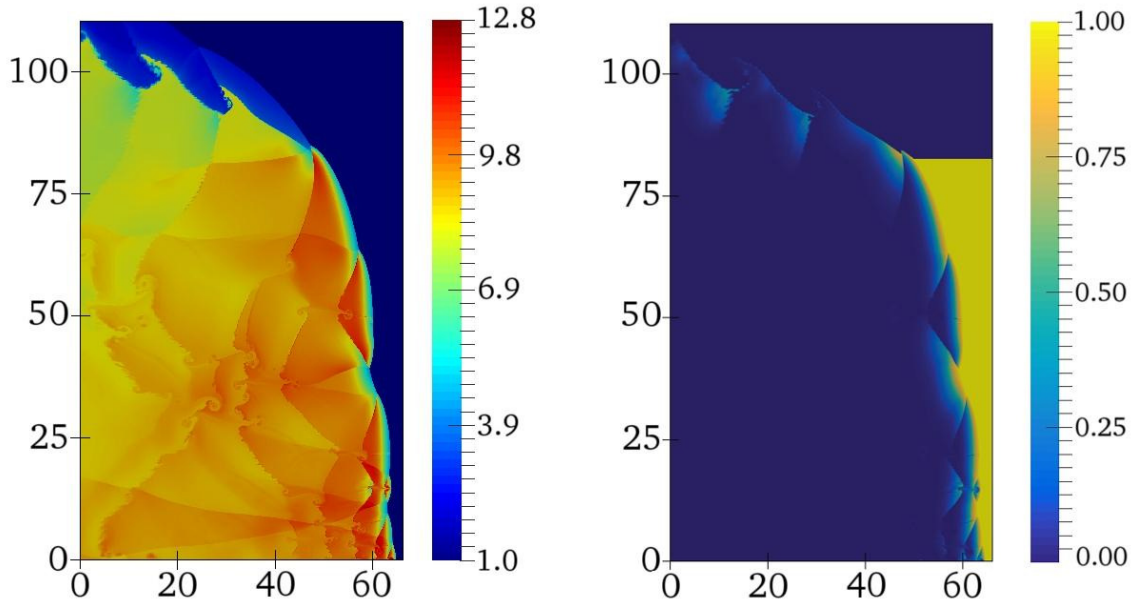

(a) Temperature T/T_0 (-)

(b) Mass fraction Y (-)

Figure 7: Propagation of a detonation-shock combined wave in a mixture with $q/rT_0 = 23.81$, $E_a/RT_0 = 20$ and $\gamma = 1.333$. The reactive layer width is $h = 7.5$ mm, i.e. $h = 82.6\ l_{1/2}$. The spatial dimensions are normalized by $l_{1/2}$.

upstream and downstream, which can be seen on the temperature field. Each of these jets generates a vortex roll on both sides of their axis. Picture (b) also indicates that a small amount of unburned gases is still persistent downstream of the detonation wave. These gas pockets are created along the detonation front when the triple points collide into each other or escape the reactive layer toward the inert medium. The pockets formed along the front are consumed in less than a cell size. The structure of the front is locally similar to the OH fluorescence images obtained by Pintgen et al.[59] for a diluted H_2-O_2 mixture.

The triple points trajectories form the cellular structure of the detonation, as depicted by the Figure 8. These numerical soot plates were obtained by saving the maximum value of pressure in cells of the most refined part of the computational domain. The upper plate relates to a detonation in a channel where the boundaries are solid walls. In this case, the cell size is small compared to the width channel to ensure that there is no acoustic coupling with the channel. The lower plate illustrates the cellular structure of the detonation-shock combined wave with a reactive layer height $h = 82.6\ l_{1/2}$. The comparison of the two figures indicates that the irregularity of the cellular structure increases as the detonation experiences

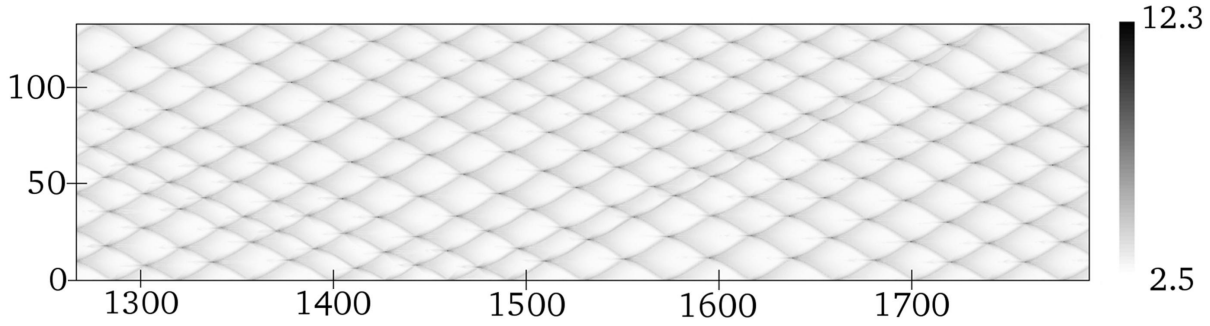

(a)

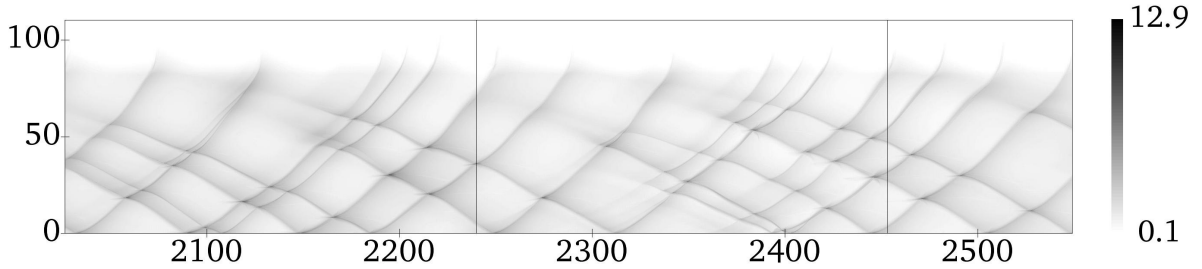

(b)

Figure 8: Maximum pressure field illustrating the cellular structure for $E_a/RT_0 = 20$. Top: Field (a) depicts the cellular structure of a detonation propagation in a channel. Bottom: Field (b) represents the cellular structure of the combined wave with $h = 7.5$ mm, i.e. $h = 82.6\ l_{1/2}$. The spatial dimensions are normalized by $l_{1/2}$ and the pressure is given in MPa.

losses. The detonation cells are enlarged by a factor of 1.5 relatively to the size obtained in the channel with solid walls. A similar behavior was reported in both experimental[32] and numerical[60] studies on the propagation of gaseous detonation in channels with porous walls. The cell axis is also deviated toward the upper part. Moreover, the Figure 8(b) reveals that the evolution of the cell size follows a cyclic pattern. During the detonation propagation, the transverse waves propagate through the interface between the reactive layer and the inert layer without any reflection. Therefore in the absence of generation of new triple points, the transverse wave number decreases and the cell size increases. The formation of new triple points only occurs when the decoupling between the incident shock and the reaction

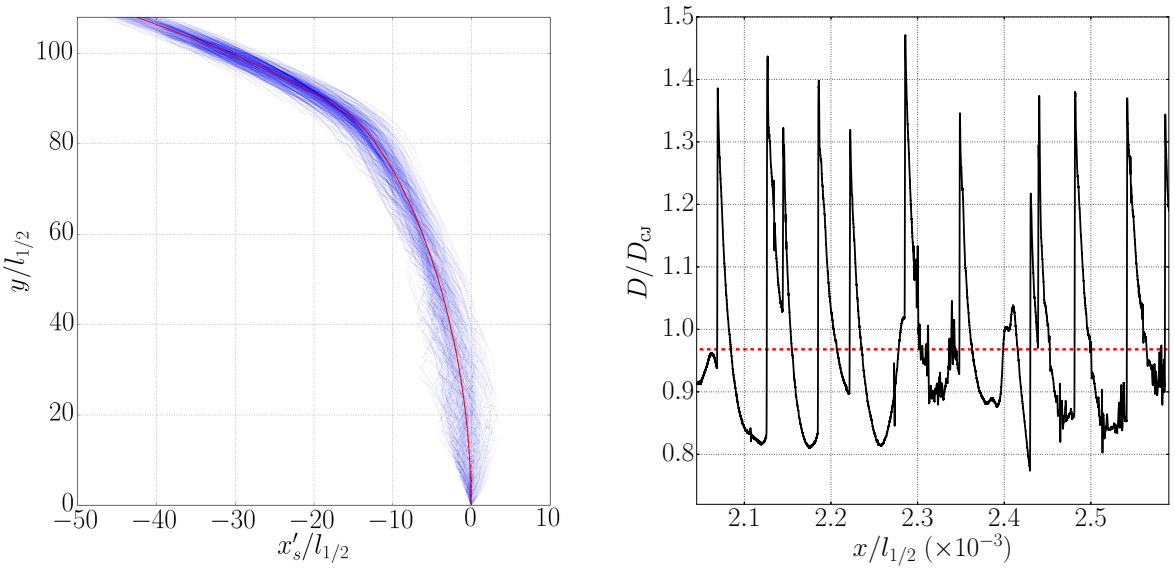

(a) (b)

Figure 9: (a) Left: Profile of the detonation-shock combined wave at different time-steps (blue) and averaged profile (red). (b) Right: Instantaneous (black) and averaged (red) velocity of the detonation measured at the bottom wall. (b) The coordinates are normalized by the half-reaction length $l_{1/2}$. The reduced activation energy is 20. The interface is located at 82.6 $l_{1/2}$.

zone appears to be imminent. At this time the detonation velocity is well short of D_{CJ}. This seems to indicate that even though the mixture is characterized by a regular cellular structure, the generation of new transverse waves is affected by the losses.

The Figure 9 (a) presents the position of each point constituting the detonation-shock combined wave at different time steps of the simulation. 250 profiles $x_s(y,t)$, extracted every 1,000 iterations, are superimposed on each other. The mean profile was calculated during the simulation by means of the averaging method introduced previously and is displayed in red. In order to facilitate the analysis, each curve $x_s(y,t)$ was plotted in the coordinates of the instantaneous position of the shock at the bottom wall, $x'_s(y,t) = x_s(y,t) - x_s(0,t)$. Because of the dynamics of the front, *i.e.* the cellular structure of the detonation, the instantaneous profiles are located on either sides of the mean curve. Due to the Prandtl-Meyer expansion centered at the intersection between the leading shock and the interface between the inert and reactive gases, the average detonation front exhibits a global curvature due to the losses.

The Figure 9 (b) also emphasizes this variability. The local velocity of the detonation measured at the bottom wall $y = 0$ and normalized by the CJ velocity is shown as a function of the distance traveled by the front. These fluctuations are ranging from 0.8 D to 1.4 D and can be correlated to the quasi-periodic impacts of the triple points against the wall. The velocity reaches a maximum during the triple point collision, then decays as the Mach stem and evolves to an incident shock. This is due to local gradients of the reactivity and to the curvature. The averaged velocity of the detonation is plotted in red and shows a deficit as compared to the CJ value.

2. $E_a/RT_0 = 30$

A greater activation energy increases the mixture sensitivity to temperature fluctuations. The reaction rate variations are wider than for stable mixtures with a lower activation energy. Thus, the flow field exhibits a more complicated structure as attested by the Figure 10. The four pictures feature a detonation propagating in a reactive layer with $h = 170.7\ l_{1/2}$. The velocity deficit is 7% as compared to the CJ velocity. As in the preceding section, the same global features can be retrieved: main curved detonation front, oblique shock front and the interface between the burned gas and the inert gas. However, these elements are much more irregular than previously observed on the combined wave with $E_a/RT_0 = 20$. The curvature variations of the front increase locally and the interface shape loses in regularity. Because of the reaction rate sensitivity to these local perturbations, the induction length between the incident shock and the onset of the exothermic reaction grows larger. Consequently, fresh gases accumulate behind the incident shock and along the shear layer, as attested by the mass fraction field. These unburnt gas pockets, which are convected downstream of the front result from the collision of triple points. The unburnt pockets are larger, more numerous and remain longer than for lower activation energies. Even if most of the unreacted material seems to be consumed within the distance of a cell size, some pockets persist throughout the end of the domain. In that case, the energy released after the characteristic line *i.e.* the sonic line does not contribute to the detonation propagation and therefore increases the velocity deficit. These pockets of fresh gases, of which boundaries are prone to increase due to the hydrodynamic instabilities, burn along their interfaces with the surrounding hotter gases and also consume in volume. These phenomena are responsible of the chaotic aspect

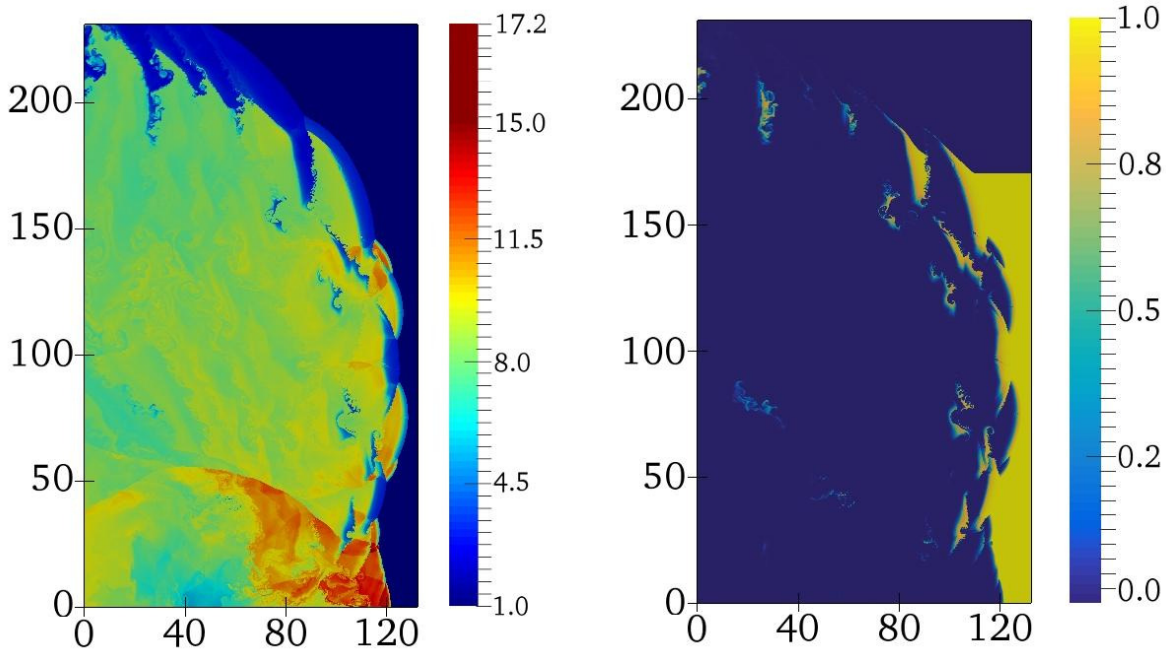

(a) Temperature T/T_0

(b) Mass fraction Y

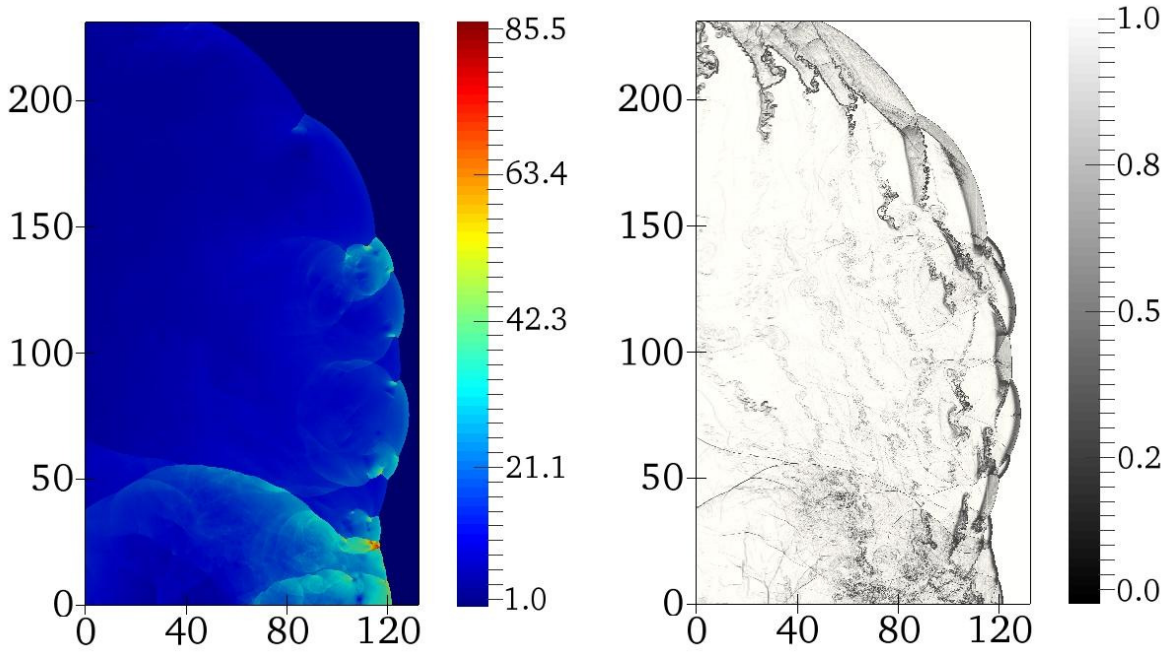

(c) Pressure P/P_0

(d) Density schlieren S

Figure 10: Propagation of a detonation-shock combined wave in mixture with $q/rT_0 = 23.81$, $E_a/RT_0 = 30$ and $\gamma = 1.333$. The reactive layer width is $h = 15.5$ mm i.e. $h = 170.7\ l_{1/2}$. The spatial dimensions are normalized by $l_{1/2}$.

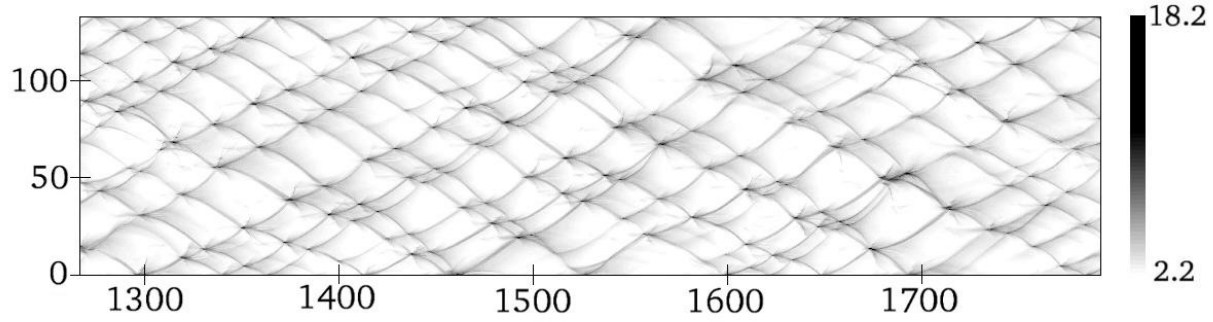

(a)

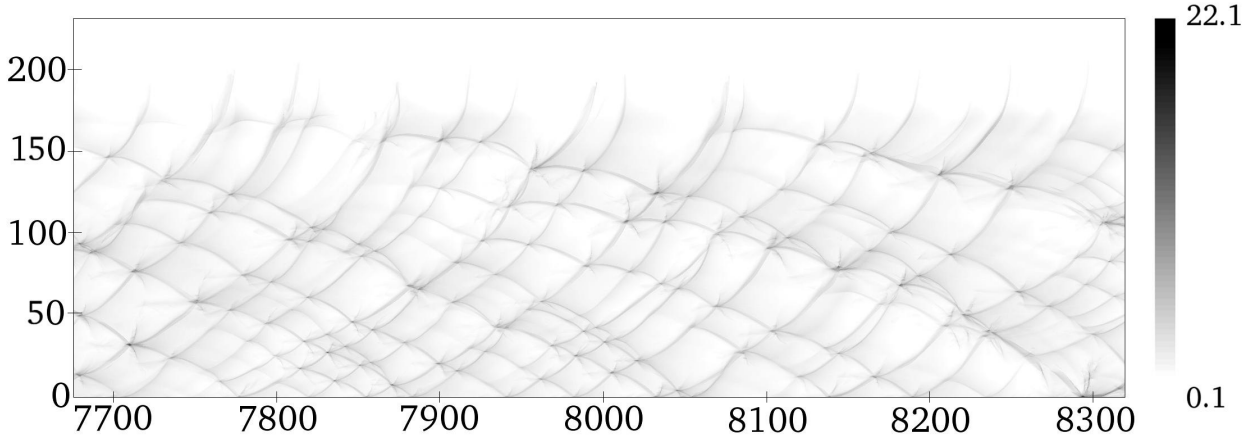

(b)

Figure 11: Maximum pressure field illustrating the cellular structure for $E_a/RT_0 = 30$. Field (a) depicts the cellular structure of a detonation propagation in a channel. Field (b) represents the cellular structure of the combined wave with $h = 15.5$ mm, i.e. $h = 170.7\ l_{1/2}$. The spatial dimensions are normalized by $l_{1/2}$ and the pressure is given in MPa.

of the flow field as it can be seen in the Figure 10 (d).

The Figure 11 shows the maximum pressure field of the detonation-shock combined wave and illustrates the cellular structure. As it was noted for a mixture with $E_a/RT_0 = 20$, the degree of irregularity of the detonation cells is increased by the presence of the inert layer, as compared to the case without loss. However, unlike the aforementioned case with a lower reduced activation energy, the average cell size does not enlarge, even if a much

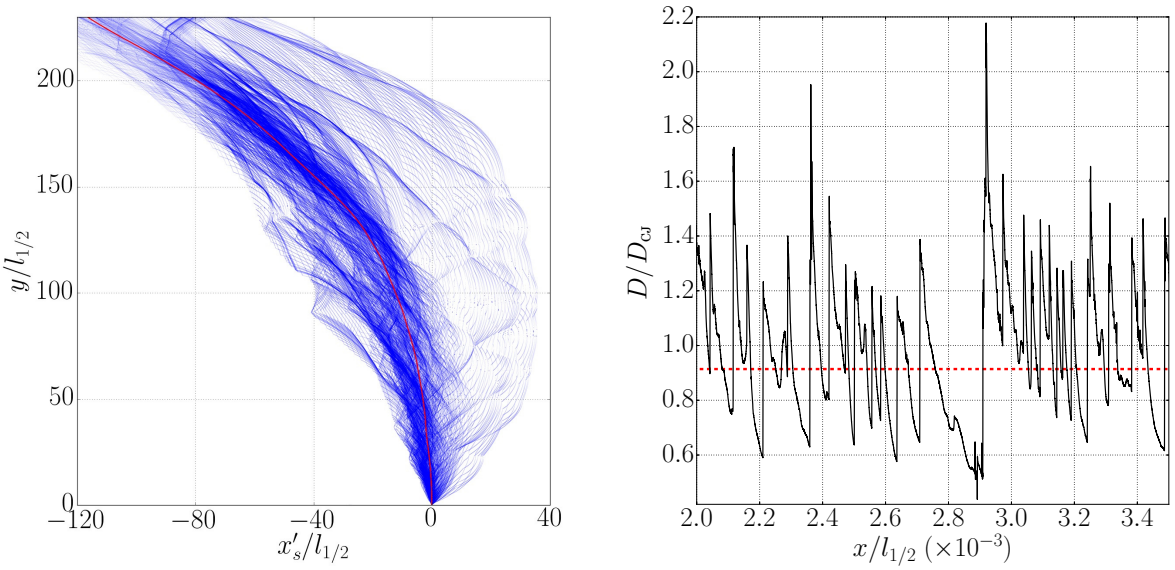

(a) (b)

Figure 12: Profiles of the detonation-shock combined wave at different time-steps (blue) and averaged profile (red). (a) Instantaneous (black) and averaged (red) velocity of the detonation measured at the bottom wall. (b) The coordinates are normalized by the half-reaction length. The reduced activation energy is 30. The interface is positioned at 170.7 $l_{1/2}$.

wider cell size spectrum can be seen. The detonation locally failed on a large part of the reactive layer, as it can be seen through the deformed and enlarged detonation cells in the lower part of the domain between the abscissa of 8050 and 8300. Nevertheless the detonation continues its propagation because of the re-initiation of new triple points on either side of the quenching area. This demonstrates the significance of the transverse waves in the sustained propagation of the detonation in an unstable mixture.

The front dynamics is illustrated in the Figure 12. The different profiles of the leading fronts are plotted in Figure 12a. As compared to the case $E_a/RT_0 = 20$, the envelope of the 2D profiles is larger. They are much more scattered around the mean value. Outside of the central core where the majority of the profiles are located, one may remark the presence of isolated profiles. They denote the existence of rare events of strong amplitude (up to two cell size) such as explosions and local failures. These profiles exhibit abrupt variations and large cusps at the triple point locations. Moreover, the detonation velocity fluctuations on Figure

12b are much higher: $0.6 \sim 1.8\bar{D}$. One can foresee local failure at $2.9 \times 10^{-3} x/l_{1/2}$ and this can be correlated to the most distant profile from the mean. These two figures illustrate the key role played by the regeneration of triple points and the associated transverse waves. The analysis of the flow field and its characterization through numerical soot plates, detonation velocity on the wall and the evolution of the detonation profiles confirm the contrast between the two families of detonation. The role played by the transverse waves differ, leading to differences in the propagation mechanism. Consequently, the effects induced by the weak confinement are different.

C. Averaged Structure

The results presented in the two previous sections highlight the prevalence of transverse wave interactions and triple point regeneration over the laminar detonation structure in the unstable mixtures. In order to quantify these discrepancies with the generalized ZND theory and to analyze the influence of the gaseous confinement, the Favre[61] averaged profiles of the detonation along the bottom wall were calculated. The Favre average of any variable ϕ is then given by

$$\widetilde{\phi} = \frac{\bar{\rho\phi}}{\bar{\rho}} \tag{11}$$

As previously mentioned, the front localization occurred via the detection of the first pressure rise. The time averaging process took place in the instantaneous leading shock frame of reference, and was achieved through the method described in the Section IV A.

The averaged profiles of the pressure ratio $\bar{p}/p_0$ are displayed in the Figure 13 for $E_a/RT_0 = 20$, $E_a/RT_0 = 30$ and $E_a/RT_0 = 38.23$, for different values of the deficit endured by the detonation. As for the mixture with the low reduced activation energy of 20, the profiles obtained as an outcome of the bidimentional simulations are close to the respective WK solutions whatever the velocity deficit endured by the detonation. Hence the effects of the weak confinement for such a stable detonation are faithfully modeled by the steady model. The residual differences between the model and the bidimensional simulations are thus only induced by the inviscid cellular structure. As the height of the reactive layer decreases, inducing more losses, the pressure field downstream of the detonation front is damped.

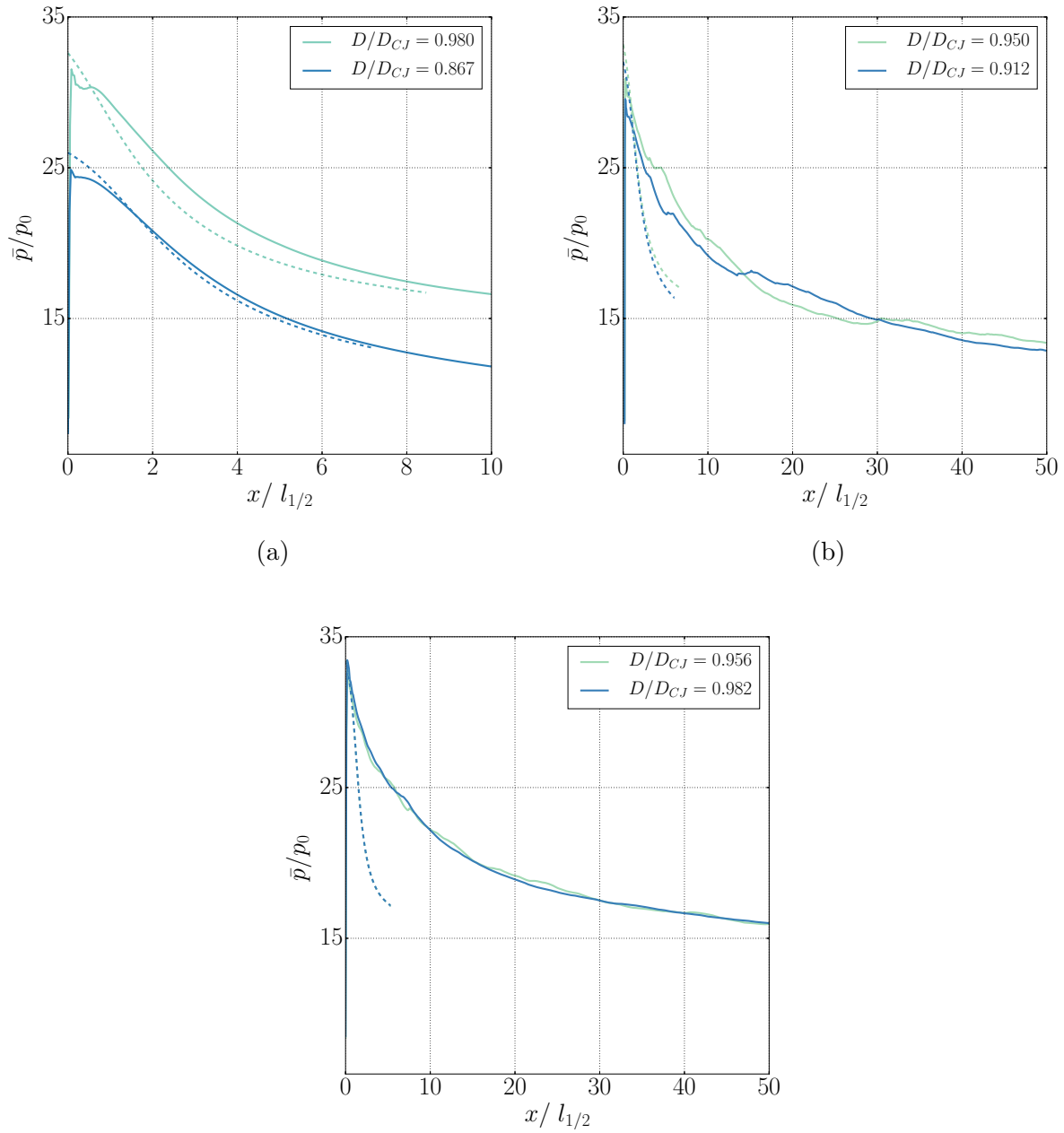

Figure 13: Average pressure profiles (solid lines) obtained for $E_a/RT_0 = 20$ (a), $E_a/RT_0 = 30$ (b) and $E_a/RT_0 = 38.23$ (c). Comparison with the WK model (broken lines).

As for the mixtures with $E_a/RT_0 = 30$ and 38.23, the differences as the losses are increased are less marked. Moreover, no similarities were obtained between the WK model and the unsteady simulations. The pressure profiles seem to have been stretched as the activation

energy is increased.

The Figure 14 shows the Favre-averaged mass fraction $\widetilde{Y}$ as a function of the distance downstream of the detonation front for different values of the activation energy and velocity deficits. Once again, very few differences exist between the unsteady results and the WK model for the mixture with $E_a/RT_0 = 20$, confirming previous findings. The weak confinement increases the distance required to perform the chemical reaction, which is consistent with the reduction of the mean pressure observed in the Figure 13. Once again, the differences increase for higher activation energies and losses. The chemical length scale has increased by a factor of almost three as compared to the one inferred by the ZND model and is lower than the cell size. The fluctuations remove part of the sensitivity of the mixture reactivity, feature highlighted by Radulescu et al.[62] for unstable detonations and by Sow et al.[57] for 1D mildly unstable detonation with losses.

The reaction zone complexity in irregular detonations challenges the validity of the length scale based on the ZND model, such as the half-reaction length. This issue led to several attempts to define new length scales that can take into account the hydrodynamic fluctuations of the reaction zone. Soloukhin[63] was the first to address this topic and to introduce the concept of hydrodynamic thickness, which differs from the classical shock reaction zone. It was defined as the distance after the leading shock beyond which the non-steady gas dynamics no longer affect the chemical and hydrodynamic processes sustaining the detonation propagation. More recently, Lee and Radulescu[64] considered the averaged position of the sonic surface as the hydrodynamic thickness boundary. By definition, in the shock coordinates, this surface propagates at $\widetilde{c}$, which ensures that any perturbation arising behind it cannot affect the reaction zone[44].We aim to investigate the evolution of this quantity along the bottom wall with the variations of the activation energy and of the reactive layer height. The Figure 15 displays the evolution of the Favre-averaged Mach number $\tilde{u}/(\gamma\bar{p}/\bar{\rho})^{1/2}$ as a function of distance from the front along with the results obtained via the WK model. For the case with $E_a/RT_0 = 20$, the length of the hydrodynamic thickness calculated with the steady model does not depart significantly from the unsteady results. The values obtained are of the same order of magnitude as those experimentally measured for the diluted mixtures[65] (up to one cell size). The increase of the velocity deficit leads to a slight reduction of the hydrodynamic thickness. Unstable detonations react in an opposite way to the weak confinement. For this type of mixture, the hydrodynamic thickness increases with the veloc-

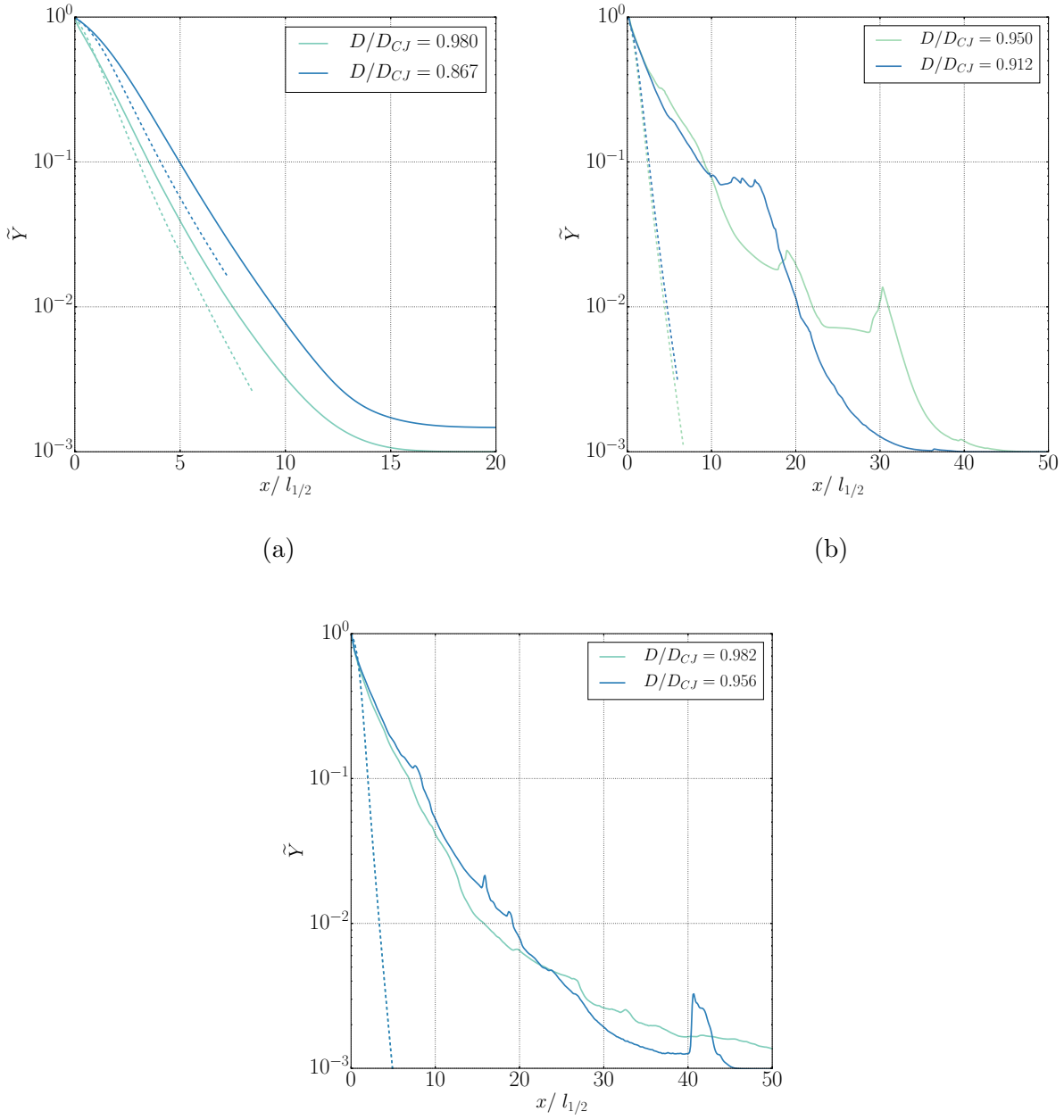

Figure 14: Average mass fraction profiles (solid lines) obtained for $E_a/RT_0 = 20$ (a), $E_a/RT_0 = 30$ (b) and $E_a/RT_0 = 38.23$ (c). Comparison with the WK model (broken lines).

ity deficit. The Table III synthesizes these results. The instabilities in irregular detonations tend to delay the position of the sonic plane. We observe an increase of the hydrodynamic thickness of one up to three times the cell size for the mildly unstable case studied here.

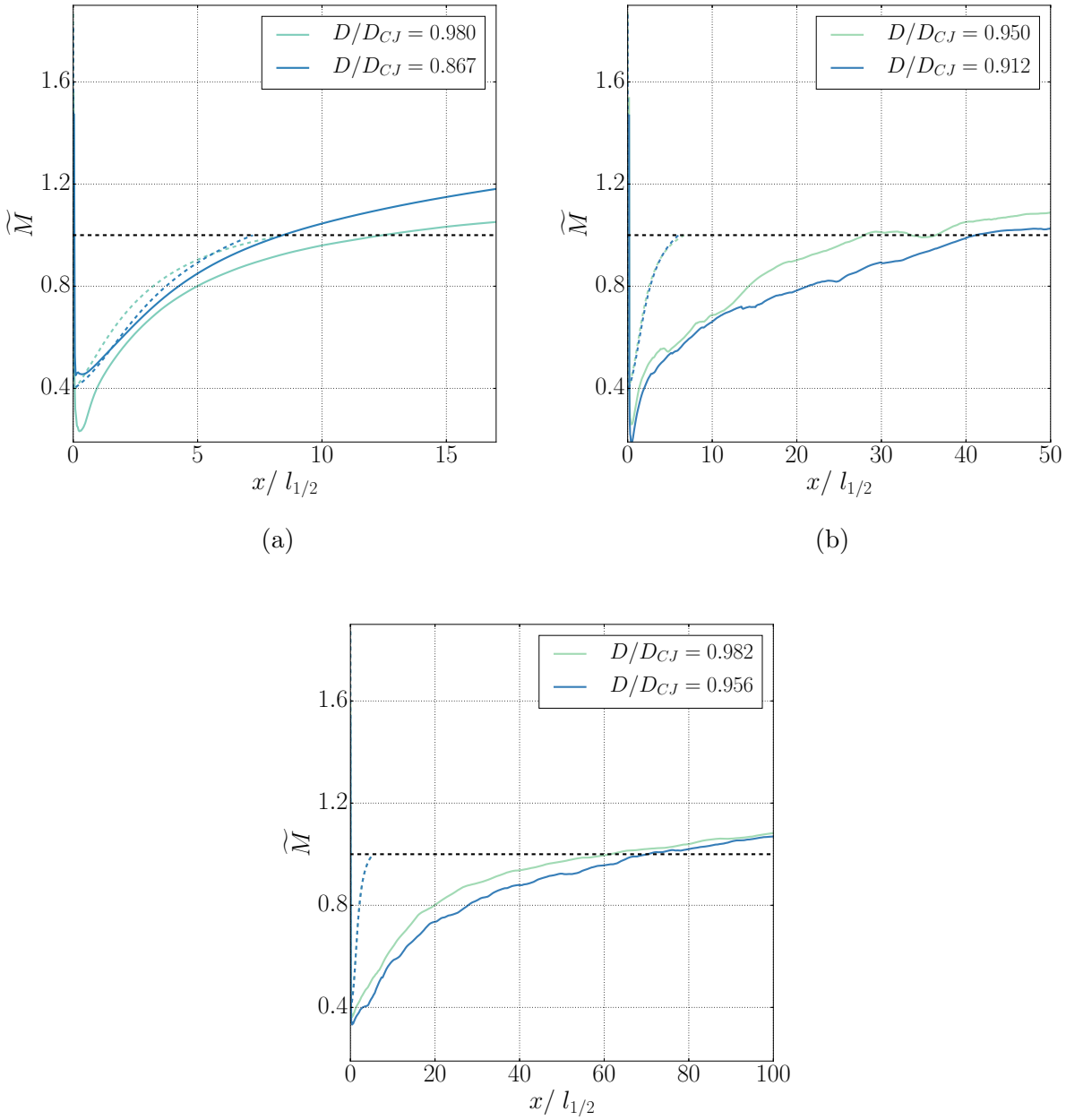

Figure 15: Average Mach number profiles (solid lines) obtained $E_a/RT_0 = 20$ (a) and $E_a/RT_0 = 30$ (b) and $E_a/RT_0 = 38.23$ (c). Comparison with the WK model (broken lines).

This trend is consistent with experimental measurements of the hydrodynamic thickness[64,66]. The increase of x_{HT} is thus mainly due to the increase of the activation energy.

In order to quantify the magnitude of these fluctuations, the Favre-average energy dis-

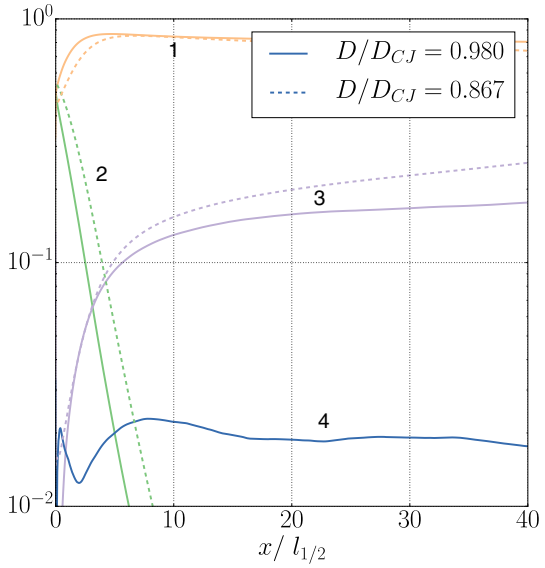

(a)

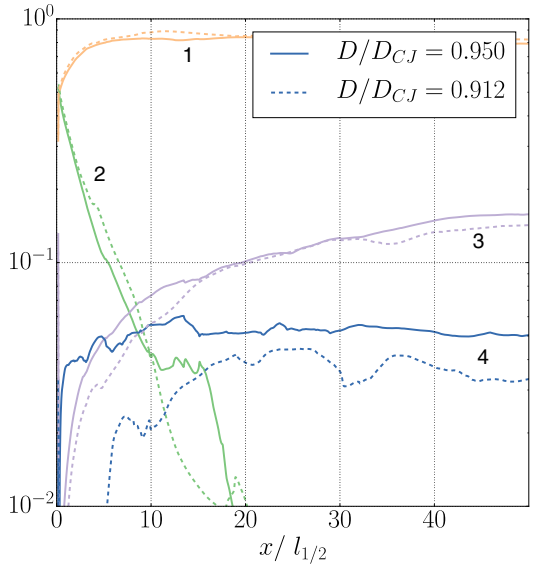

(b)

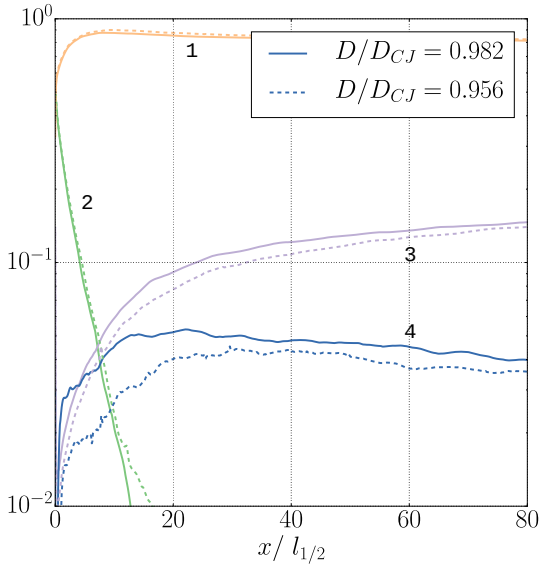

(c)

Figure 16: Average energy repartition obtained for $E_a/RT_0 = 20$ (a), $E_a/RT_0 = 30$ (b) and $E_a/RT_0 = 38.23$ (c). Internal energy (curve 1), chemical energy (curve 2), kinetic energy (curve 3) and energy of the mechanical fluctuations (curve 4). The latter have been normalized by the total energy.

D/D_{CJ}	$E_a/RT_0 = 20$	$E_a/RT_0 = 30$	$E_a/RT_0 = 38.23$
$D_{\mathrm{lim}}/D_{\mathrm{CJ}}$	0.45	1.77	3.3

Table III: Values of the normalized hydrodynamic thickness x_{TH}/λ obtained for the critical velocity deficit and different activation energies from unsteady simulations.

tributions presented in the Figure 16 describe the relative contribution of each term of the energy conservation equation following the approach of Radulescu et al.[62]. The internal energy is $\widetilde{e}$, the chemical energy $\widetilde{Y}q$, the kinetic energy is $(\widetilde{u}^2 + \widetilde{v}^2)/2$, which simplifies to $\widetilde{u}^2/2$ on the wall. The energy of the mechanical fluctuations refers here to $k = (\widetilde{u"^2} + \widetilde{v"^2})/2$, which is equal to $\widetilde{u"^2}/2$ on the wall, as the spanwise velocity is zero on the wall. The latter k is computed as $\widetilde{E} - \widetilde{u}^2/2 - \widetilde{e} - \widetilde{Y}q$. The kinetic energy continues to grow as the Mach number of the mean flow increases. The chemical length related to the completion of the reaction increases with the activation energy and varies from 0.2 λ to 0.7 λ. The energy carried by the fluctuations grows through the subsonic zone, and remains stable after the sonic locus. According to the mixture stability, the relative part of the fluctuations rises from 1% to 4.5% to the detriment of the kinetic and internal energies.

These findings corroborate the existence of a distinct propagation mechanism for the more unstable mixtures. As the mixture gains in instability, the hydrodynamic thickness as well as the reaction length increase. Moreover, the influence of the weak confinement leads to different effects according to the regularity of the cellular structure. In particular, the hydrodynamic thickness is reduced by the weak confinement in the case of stable detonations whereas for unstable mixtures this distance increases slightly. One may also remark that despite the intensity of hydrodynamic fluctuations at the center of the cell, the energy of the mechanical fluctuations remains relatively weak behind the shock.

D. Failure mechanisms

We further analyzed the flow fields to study the mechanisms accounting for the detonation failure when the reactive layer height is suddenly decreased below the critical value h_{lim}. In order to catch this transient phenomenon, the detonation propagated first in a gaseous layer slightly larger than the critical height. Then, when a mean detonation velocity was reached,

the reactive layer height was reduced under the critical value h_{lim}. From that moment on, the detonation quenched more or less quickly depending on the detonation stability.

As for the mixtures characterized by $E_a/RT_0 = 10$ and 20, the flow field is fully laminar for reactive layer heights close to the critical value and the cellular structure is absent. Thus, the flow divergence coming from the interactions with the inert layer only acts on the frontal curvature. When the reactive layer height becomes too small, the curvature progressively increases until a global decoupling of the reaction zone from the leading shock occurs. The simulation was performed with reactive layer heights from $h = 3.5$ mm to $h = 2.5$ mm for $E_a/RT_0 = 20$.

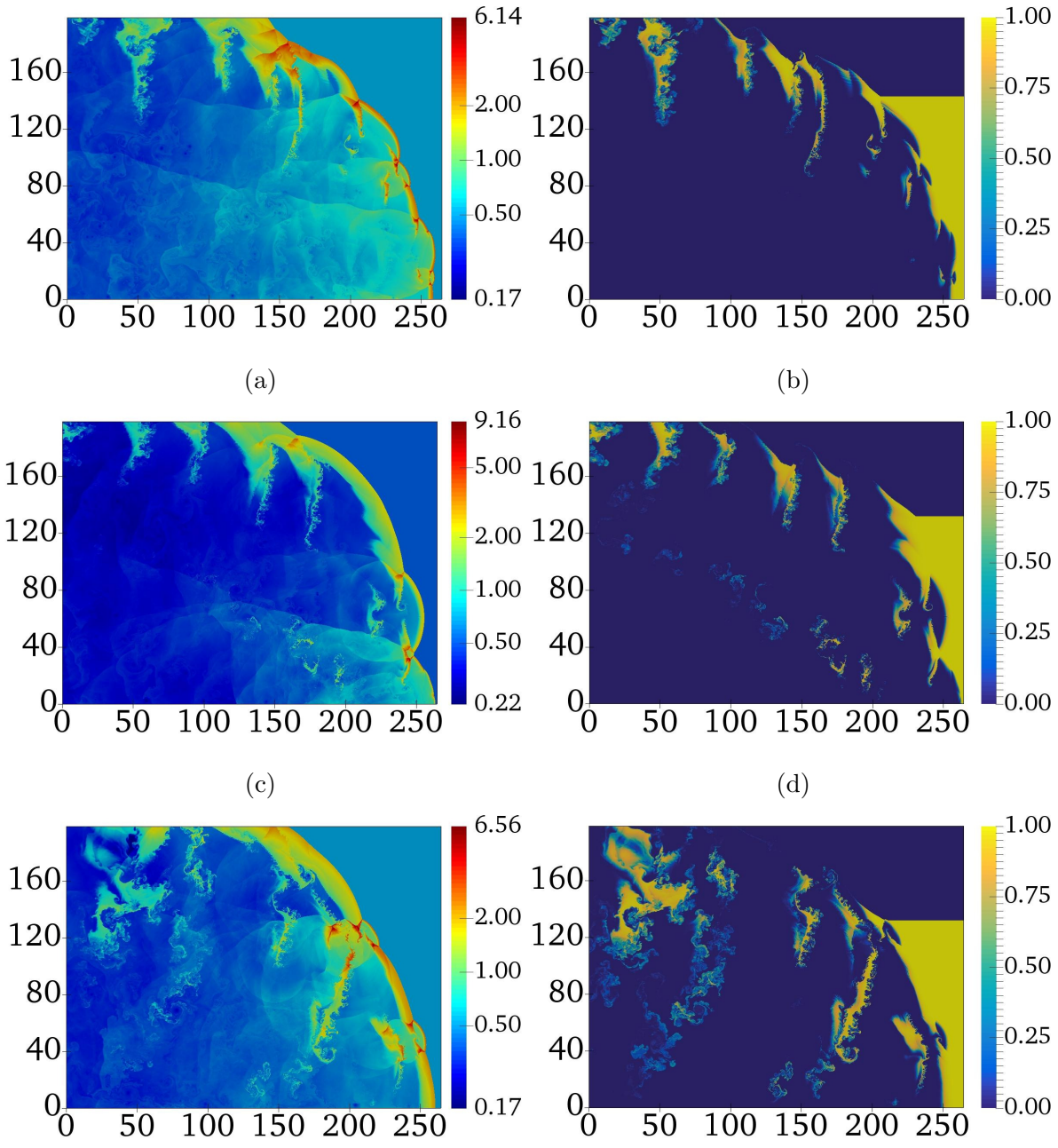
0
40
80
120
160
0 50 100 150 200 250
6.14
2.00
1.00
0.50
0.17
1.00
0.75
0.50
0.25
0.00
9.16
5.00
2.00
1.00
0.50
0.22
6.56
2.00
1.00
0.50
0.17
1.00
0.75
0.50
0.25
0.00

(a) (b)

(c) (d)

(e) (f)

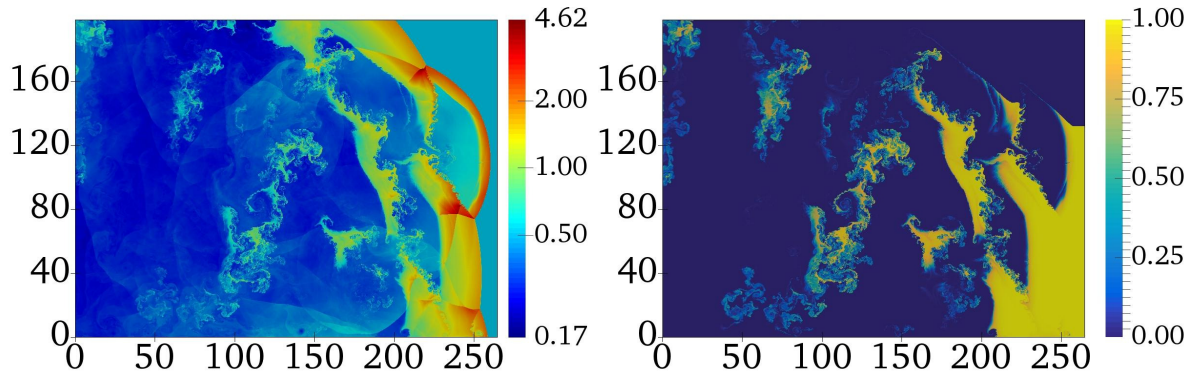

(g) (h)

Figure 17: Propagation and failure of a detonation-shock combined wave in a mixture with $q/rT_0 = 23.81$, $E_a/RT_0 = 30$ and $\gamma = 1.333$. Fields of density normalized by ρ_0 (left, logarithmic scale) and mass fraction (right). The reactive layer width is initially $h = 13.5$ mm i.e. $h = 148.7\ l_{1/2}$ and is reduced to $h = 12.5$ mm i.e. $h = 137.6\ l_{1/2}$. The spatial dimensions are normalized by $l_{1/2}$

For higher activation energies (*i.e.* $E_a/RT_0 = 30$ and 38.23), transverse waves are present whatever the reactive layer height. The divergence losses influence not only the overall curvature of the front, but also the irregular cellular structure of the detonation. We carried out with a simulation with reactive layer height decreasing from $h = 13.5$ mm to $h = 12.5$ mm for $E_a/RT_0 = 30$. The Figure 17 presents the evolution of the detonation-shock combined wave as the failure occurs. The two first frames depict the detonation propagating in the reactive layer before the height reduction. As the reactive layer height is suddenly decreased, the cell size increases as well as the distance between the incident shock and the reaction zone. Consequently, a larger amount of gas is torn off from the front during the triple point collisions. Then the number of non-reacted gas pockets, their size and their depth of penetration increase progressively. As most of the pocket burning process occurs beyond the sonic line, their combustion does not contribute anymore to the detonation propagation. Ultimately, there is a local decoupling and the transverse waves are not able to initiate the detonation on one part of the front, as it can be seen in the Figure 17 (h). In this frame the lower part of the detonation is quenched, whereas the upper part continues its propagation. Finally, the failure extends on the whole front. The cellular structure associated to this sequence is shown in the Figure 18. Once the reactive layer height is decreased below

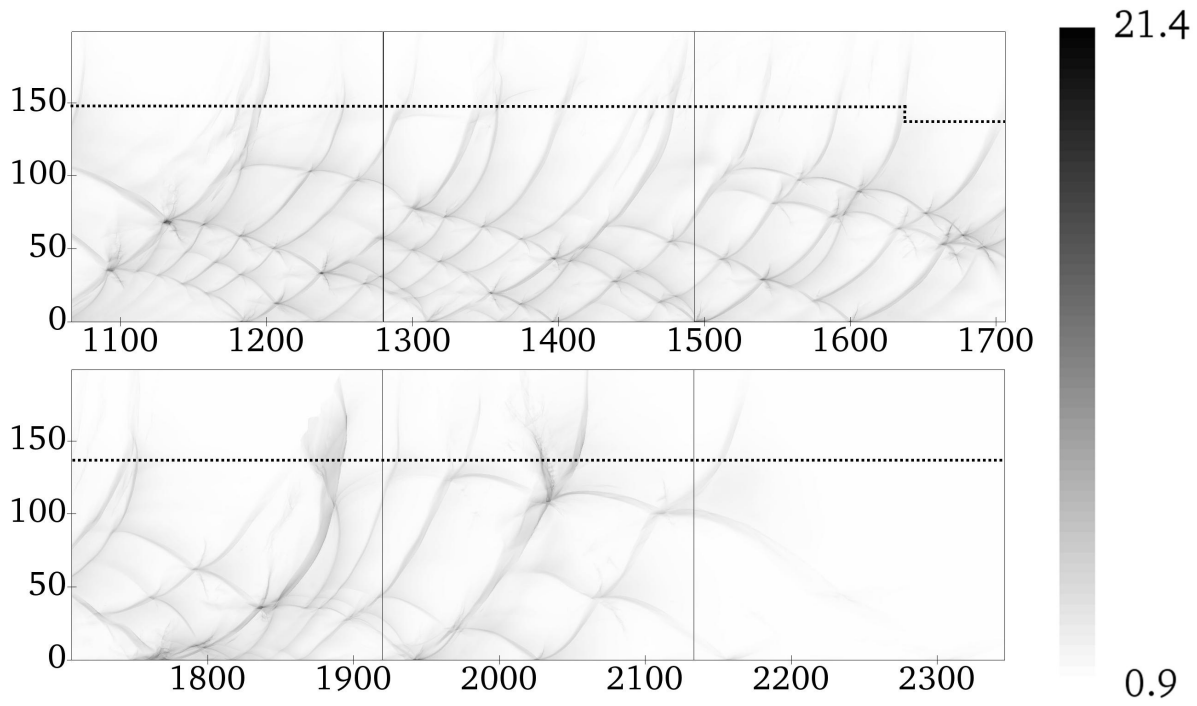

Figure 18: Maximum pressure field illustrating the cellular structure of a detonation undergoing failure for $E_a/RT_0 = 30$. The spatial dimensions are normalized by $l_{1/2}$ and the pressure is given in MPa. The position of the interface (dotted line) is initially $h = 13.5$ mm i.e. $h = 148.7\ l_{1/2}$ and is reduced to $h = 12.5$ mm i.e. $h = 137.6\ l_{1/2}$. Each field corresponds to a different instant.

h_{lim}, the rate of generation of new triple points slowly decays, leading to the failure of the detonation. The cellular structure disappears over a distance of approximately 20 λ. This length seems to be of the same order than the back-and-forth trajectory followed by the transverse waves starting from the interface toward the bottom wall. This could indicate that the information about the height of the reactive layer, and thus about the failure, is propagated by means of the transverse waves.

The study of the failure process occurring when the losses become too strong confirms the significance of the transverse waves for the unstable mixtures. Our simulations shows that in this case, as the height of the reactive layer became smaller, the generation rate of new triple point was insufficient to prevail over the detonation quenching. Radulescu and Lee[32] supported this observation through the analysis of open shutter photographs. For the

argon diluted mixture, they associated the detonation failure to the progressive increase of the front curvature whereas for the unstable mixture the elimination of transverse waves was at the root of the quenching process.

V. DISCUSSION

The simulation of detonations confined by an inert gas layer for several activation energies has confirmed the existence of two different behaviors concerning the detonation propagation. In our study, the results obtained from the WK model and from the numerical simulations greatly differ according to the stability of the mixture. While keeping the half-reaction length constant, the irregularity of the cellular structure was controlled through the value of the activation energy. Moen et al.[67] were among the first to put in doubt the universality of the detonation behavior. They performed velocity measurement for detonations propagating in tubes of various diameters. The results obtained for argon-diluted mixtures were remarkably predicted by Fay's theory unlike non-diluted mixtures. Comparable studies[68–70] led to similar results, as well as experimental investigations related to the detonation propagation in tubes with porous walls[32]. The consistency of the models for the diluted mixtures with a regular cellular pattern indicates that a shock compression followed by an exothermic reaction adequately describes the propagation mechanism in this case.
The adequacy between the WK model and the numerical results for low activation energy confirms this propagation mechanism. For low activation energy - very regular and weakly unstable detonations - all the curves match the WK model (see Figure 5). As the activation energy is increased, more modes of longitudinal instabilities are activated and the departure from the WK model is then clear. When losses are present, we can notice that as the velocity deficit increases, the cell irregularity grows. This is consistent with experimental findings concerning detonations subjected to losses via porous walls[32]. Moreover, the scaling -detonation velocity vs. curvature breaks down even if the half-reaction length and the cell sizes are roughly the same for the two mildly unstable cases investigated here.

As for the hydrodynamic thickness, the values derived from the numerical simulations are in line with experiments[65,71]. They increase with the cell irregularity, as well as with the losses, which is also coherent with experimental findings. The numerical results also show that their variation is more pronounced with the increase of the cell irregularity than

with losses. Indeed, the presence of the mechanical and thermal fluctuations delayed the averaged sonic boundary far from the end of the main heat-release reaction zone. The end of the mean subsonic reaction zone thus corresponds to the stabilization of the production of these fluctuations and the presence of a small heat-release zone. We have also shown from the mean profiles along the bottom wall, that the subsonic zone has been lengthened as compared to the WK model. Moreover, the chemical length gets thicker. This suggests that the fluctuations have removed part of the sensitivity of the mixture reactivity to temperature. However, the increase of the cell size due to losses is not as stringent as in the recent experiments of Jarsalé et al.[72], even if the losses were volumetric and induced by the presence of a spray of fine water droplets.

The detonation front presents a global curvature coming from the Prandtl-Meyer expansion, which depends on the height of the reactive layer. The detonation front consists of many sections which are locally convex towards the upstream flow[30]. They are deviated towards the averaged leading curved detonation front. As E_a is increased, rare events of stronger amplitude appear. The leading front is composed of fewer sections of larger convexity. The propagation of unstable detonations is a succession of local failures and pointwise explosions (see Figure 12). Indeed, the reaction zone progressively draws away from the shock, until a transverse wave reinitiates the exothermic reaction. Regeneration of new triple points and transverse waves can be correlated with the greater bulbs and more pronounced cusps of the detonation profiles as well as the greater excursions from the mean of the detonation velocity. The amplitude of these events, as well as their regularity are directly linked to the activation energy and to the losses to a smaller extent.

The importance of these transverse waves has also been highlighted in §IV D. The decay of the detonation front up to failure seems to be diffusion-like for detonations with low activation energy[73], as the decay occurs in a very progressive manner. In this case, the failure is uniquely due to the front curvature. In the case of unstable detonations, the quenching arises more suddenly as the information of the expansion from the top layer was brought by discrete transverse wave collisions down to the bottom wall.

In the present study, the minimal height of the reactive layer allowing the successful propagation of the detonation increases with the activation energy. However, various results from experimental investigations suggest that as the losses endured rise, unstable detonations are more robust than regular ones. For instance, it has been shown that successful

transmission of the detonation in an unconfined space depends on the mixture regularity[10]. The argon-diluted mixtures follow a $d_c/\lambda \simeq 20 \sim 30$ correlation whereas the unstable ones behave according to a $d_c/\lambda \simeq 13$ correlation. Experimental study with porous wall effects by Radulescu and Lee are also in line with this conclusion. They obtained a critical channel height smaller for unstable mixtures than for diluted-regular ones. A similar trend was noticed in studies addressing the influence of the boundary layer on a detonation propagating in small diameter tubes[68–70]. However, the critical height (20λ) obtained in our simulations for the most unstable mixture approaches the upper limit of the sizing rule recommended by Bykovskii et al[2]. They stated that the minimal height of fresh mixture in a rotating detonation engine must range between $(12 \pm 5)\lambda$ to ensure the propagation of a detonation wave. Although most of the other experimental studies[15,18,21,23–26,74,75] concerning detonations bounded by an inert layer indicated a much lower limit, the experimental conditions such as the nature of the inert boundary, the geometry of the experiment or the presence of a film at the interface might affect the results. If the thickness of the film separating the reactive and inert layers is too large, it partially acts as a rigid interface of which the inertia cannot be neglected in the detonation dynamics[76,77]. Experimental results of the same order of magnitude than in our study were obtained for free columns of reactive gases without any film[22,76,78]. The rate of gasdynamic expansion also depends on the experimental apparatus: the losses are more important in the case of a cylindrical free charge without any solid boundary than for a rectangular channel with three solid walls and one free boundary. All these differences between the experiments make it difficult to comprehend the predictive quality of the simulation results.

As for the different trends between stable and unstable mixtures, most numerical investigations on this topic reach the same conclusions as our numerical results. Sow et al.[57] performed one-dimensional simulations of mildly unstable detonation with friction losses. They showed that as the diameter of the tube decreases, pulsating detonations are more subject to failure than the stable ones. The critical diameter under which quenching was observed increased with the activation energy. A similar behavior has been encountered by Mazaheri et al.[60] in their numerical study of detonations propagating in a porous tube. In an argon-diluted mixture, the failure occurred with one detonation cell present within the flow field whereas for non-diluted mixtures the quenching arose with the presence of several transverse waves. One exception is that of Li et al.[29], where the detonation resilience to

failure was enhanced with the presence of upstream initial heterogeneities, even though the chosen kinetics and thermodynamic parameters did not ensure the intrinsic development of the cellular structure.

In our study, E_a/RT_0 was the sole parameter which controls the level of the cell irregularity. From the classification of Strehlow[30], we can say that it ranges from the excellent to the poor cases. There are great similarities between the phenomenology brought about the numerical results and experimental findings, even if experiments also referred to more irregular mixtures with substructures, which are more sensitive to temperature fluctuations. In our simulations, the velocity deficit increases with the activation energy, as illustrated in the Figure 6. Moreover, elements relative to the near-limit behavior are not reproduced, in particular the robustness of unstable detonation in comparison with stable ones. As E_a is increased, the cell size remains roughly constant, but the irregularity increased with a wider spectrum of cell sizes. This means that the reservoir of hot spots is increased. Nevertheless, this is not sufficient to balance the losses and to prevent quenching. Indeed, the discrete transverse wave collisions transport efficiently the losses coming from the top layer expansion. However, the corresponding hot spots are not energetic enough and not sufficiently sensitive to the temperature fluctuations, as overall the pressure waves which run through the subsonic zone and hydrodynamic fluctuations also act to remove part of the thermal sensitivity of the mixture. The transverse waves are here inefficient to reinitiate the detonation. The difficulties to retrieve the behavior at detonation limits in the case of unstable detonations, can be due to the shortcomings of the model employed[58]. Three-dimensional effects can be expected, as this can enhance the occurrence of hot spots and thus the probability of reinitiating the detonation. This is a critical issue for the proper comparison with the experiments in rectangular channels, in which transverse waves are propagating in the third dimension. Another probable reason could be due to the burning mechanism. Althought the most irregular mixture of the study is only mildly unstable, it has been shown that the losses play a destabilizing role in the dynamics of detonation[55,79]. Unstable detonation feature layers, ligaments of fresh gases which burn as shock-compressed pockets of gases detached from the leading shock via nonequilibrium reactive compressible turbulence[80,81], shock-shock and shock-vortex interactions. These phenomena are amplified near the limits of propagation.

The existence of these pockets was reported in numerous experimental investigations.

Subbotin[82] was the very first to observe islands of unburnt gases behind the detonation front. This was confirmed through the study of Austin et al[83], who visualized the pockets by the means of OH fluorescence images. They were seen to be consumed within the distance of one cell size[62]. Kiyanda et al.[80] performed high-speed Schlieren and self-emitted light photographs in highly irregular mixtures and demonstrated that 40% of the fresh gases engulfed in pockets of unburned gases, are consumed via turbulent mixing between hot and cold gases. This is enhanced by the presence of hydrodynamic instabilities (Richtmyer-Meshkov, Rayleigh-Taylor, Kelvin-Helmholtz)[62,84,85]. This analysis questions the suitability of the Euler equations concerning the simulations of very highly unstable detonations. The unburnt pockets combustion exclusively occurs via the numerical diffusion, and hence depends on the calculation resolution as well as the order of the scheme used. The role played by the diffusion in the detonation propagation was addressed in several papers[86–88]. The large-scale coherent structures, small-scale elements and the mixture sensibility may influence the burning delay of the unreacted pockets and therefore the propagation limits of the detonation. However, the implementation of the Navier-Stokes equations in order to get more physical results is not straightforward. Indeed, it has been shown that a very high resolution in needed in order to fully resolve the scales present within the flow field[62]. Less than 300 points per half reaction length lead to results similar to the Euler equations outcome[86]. Such a resolution, which is one order of magnitude larger than the one employed in the present manuscript, is beyond our computational capabilities and would prevent from performing this parametric study.

As far as the cell structure is not highly irregular, the reactive Euler equations can be used. Indeed, mean quantities such as the detonation velocity, the global curvature, the pressure and the Mach number profiles are barely affected.

VI. CONCLUSION

This numerical study takes an interest in the role played by a gaseous boundary on the detonation propagation. Mixtures of various activation energies were investigated from a very regular to a mildly unstable which corresponds to a stoichiometric hydrogen—oxygen mixture at one atm. The detonation evolved in reactive layers of different heights to vary the losses endured by the front. The influence of the inert confinement differs according to

the mixture sensitivity. The WK model is relevant in the case of low activation energies but not for the weakly unstable ones. Major discrepancies in the propagation mechanism are at the root of these differences. In unstable mixtures, the generation of new triple points is the keystone allowing the propagation of self-sustained detonations. Moreover, non-negligible amount of unburnt gases are convected downstream of the front, enhancing the flow field complexity in the course of their combustion. These intrinsic features of mildly unstable detonations were satisfactorily simulated in the numerical results. The analysis of the flow field and the Favre averaged quantities along the bottom wall are in accordance with the experimental findings: the velocity deficit increases with the cellular structure irregularity and the values of the hydrodynamic thickness are in agreement with the ones derived from experiments. The critical height of propagation is found to be in line with the criterion calculated by Bykovskii et al.[2]. However, the discussion in relation to other detonation experiments with losses questions the specificity of this configuration, how the regeneration of transverse waves can enhance the detonation resistance to failure, as well as the models employed in the case of highly unstable mixtures.

ACKNOWLEDGMENTS

The computations were performed using HPC resources from the cluster of Pprime, the Mésocentre de Calcul Poitevin and from GENCI-CINES (Grant 2016-c20162b7735). This work is part of the CAPA research program on Alternative Combustion Mode for air-breathing Propulsion supported by SAFRAN Tech, MBDA France and ANR (National Research Agency).

REFERENCES

[1]K. Kailasanath, "Review of propulsion applications of detonation waves," AIAA Journal **38**, 1698–1708 (2000).

[2]F. A. Bykovskii, S. A. Zhdan, and E. F. Vedernikov, "Continuous spin detonations," Journal of Propulsion and Power **22**, 1204–1216 (2006).

[3]M. Hishida, T. Fujiwara, and P. Wolański, "Fundamentals of rotating detonations," Shock Waves **19**, 1–10 (2009).

[4]D. Schwer and K. Kailasanath, "Numerical investigation of the physics of rotating-detonation-engines," Proceedings of the Combustion Institute **33**, 2195 – 2202 (2011).

[5]P. Wolański, "Detonative propulsion," Proceedings of the Combustion Institute **34**, 125 – 158 (2013).

[6]W. Fickett and W. C. Davis, *Detonation: theory and experiment* (Courier Corporation, 2012).

[7]Y. Zel'dovich, "On the theory of the propagation of detonation in gaseous systems," Zh. Eksp. Teor. Fiz. (Journal of Experimental and Technical Physics) **10**, 542–568 (1940).

[8]J. A. Fay, "Two-dimensional gaseous detonations: Velocity deficit," Physics of Fluids **2**, 283–289 (1959).

[9]A. Chinnayya, A. Hadjadj, and D. Ngomo, "Computational study of detonation wave propagation in narrow channels," Physics of Fluids (1994-present) **25**, 036101 (2013).

[10]J. H. S. Lee, *The detonation phenomenon* (Cambridge University Press, 2008).

[11]H. Jones, "A theory of the dependence of the rate of detonation of solid explosives on the diameter of the charge," Proceedings of the Royal Society of London A: Mathematical, Physical and Engineering Sciences **189**, 415–426 (1947).

[12]H. Eyring, R. E. Powell, G. H. Duffy, and R. B. Parlin, "The stability of detonation," Chemical Reviews **45**, 69–181 (1949).

[13]W. W. Wood and J. G. Kirkwood, "Diameter effect in condensed explosives. the relation between velocity and radius of curvature of the detonation wave," The Journal of Chemical Physics **22**, 1920–1924 (1954).

[14]J. B. Bdzil, "Steady-state two-dimensional detonation," Journal of Fluid Mechanics **108**, 195–226 (1981).

[15]W. P. Sommers, "Gaseous detonation wave interactions with nonrigid boundaries," ARS Journal **31**, 1780–1782 (1961).

[16]W. P. Sommers and R. B. Morrison, "Simulation of condensed-explosive detonation phenomena with gases," Physics of Fluids **5**, 241–248 (1962).

[17]E. K. Dabora, "The influence of a compressible boundary on the propagation of gaseous detonations," Tech. Rep. 3559-E (NASA, 1963).

[18]E. K. Dabora, J. A. Nicholls, and R. B. Morrison, "The influence of a compressible boundary on the propagation of gaseous detonations," (Combustion Institute, Pittsburgh, 1965) pp. 817 – 830.

[19]T. G. Adams, Ph.D. thesis, Michigan State University (1972).

[20]T. G. Adams, "Do weak detonation waves exist?" AIAA Journal **16**, 1035–1040 (1978).

[21]S. B. Murray and J. H. S. Lee, "The influence of yielding confinement on large-scale ethylene-air detonations," Progress in Astronautics and Aeronautics **94**, 80–103 (1984).

[22]A. A. Vasil'ev and D. V. Zak, "Detonation of gas jets," Combustion, Explosion and Shock Waves **22**, 463–468 (1986).

[23]W. Rudy, M. Kuznetsov, R. Porowski, A. Teodorczyk, J. Grune, and K. Sempert, "Critical conditions of hydrogen-air detonation in partially confined geometry," Proceedings of the Combustion Institute **34**, 1965–1972 (2013).

[24]W. Rudy, M. Zbikowski, and A. Teodorczyk, "Detonations in hydrogen-methane-air mixtures in semi confined flat channels," Energy **116, Part 3**, 1479 – 1483 (2016).

[25]W. Rudy, K. Dziubanii, M. Zbikowski, and A. Teodorczyk, "Experimental determination of critical conditions for hydrogen-air detonation propagation in partially confined geometry," International Journal of Hydrogen Energy , 4–11 (2016).

[26]J. Grune, K. Sempert, A. Friedrich, M. Kuznetsov, and T. Jordan, "Detonation wave propagation in semi-confined layers of hydrogen–air and hydrogen–oxygen mixtures," International Journal of Hydrogen Energy **42**, 7589 – 7599 (2017).

[27]V. N. Gamezo and E. S. Oran, "Reaction-zone structure of a steady-state detonation wave in a cylindrical charge," Combustion and flame **109**, 253–265 (1997).

[28]J. Li, X. Mi, and A. J. Higgins, "Geometric scaling for a detonation wave governed by a pressure-dependent reaction rate and yielding confinement," Physics of Fluids **27** (2015).

[29]J. Li, X. Mi, and A. J. Higgins, "Effect of spatial heterogeneity on near-limit propagation of a pressure-dependent detonation," Proceedings of the Combustion Institute **35**, 2025 – 2032 (2015).

[30]R. A. Strehlow, "Gas phase detonations: Recent developments," Combustion and Flame **12**, 81 – 101 (1968).

[31]J. C. Libouton, A. Jacques, and P. J. Van Tiggelen, "Cinétique, structure et entretien des ondes de détonation," Actes du colloque international Berthelot-Vieille-Mallard-Le Chatelier **2**, 437–442 (1981).

[32]M. I. Radulescu and J. H. S. Lee, "The failure mechanism of gaseous detonations: experiments in porous wall tubes," Combustion and Flame **131**, 29 – 46 (2002).

[33]G. J. Sharpe, "Transverse waves in numerical simulations of cellular detonations," Journal of Fluid Mechanics **447**, 31–51 (2001).

[34]D. A. Kessler, V. N. Gamezo, and E. S. Oran, "Multilevel detonation cell structures in methane-air mixtures," Proceedings of the Combustion Institute **33**, 2211–2218 (2011).

[35]B. Khasainov, F. Virot, H.-N. Presles, and D. Desbordes, "Parametric study of double cellular detonation structure," Shock Waves **23**, 213–220 (2013).

[36]B. D. Taylor, D. A. Kessler, V. N. Gamezo, and E. S. Oran, "Numerical simulations of hydrogen detonations with detailed chemical kinetics," Proceedings of the combustion Institute **34**, 2009–2016 (2013).

[37]V. N. Gamezo, D. Desbordes, and E. S. Oran, "Two-dimensional reactive flow dynamics in cellular detonation waves," Shock Waves **9**, 11–17 (1999).

[38]V. N. Gamezo, D. Desbordes, and E. S. Oran, "Formation and evolution of two-dimensional cellular detonations," Combustion and Flame **116**, 154 – 165 (1999).

[39]M. Kaneshige and J. E. Shepherd, "Detonation database," Tech. Rep. FM97-8 (GALCIT, 1997).

[40]A. Suresh and H. T. Huynh, "Accurate monotonicity-preserving schemes with runge–kutta time stepping," Journal of Computational Physics **136**, 83 – 99 (1997).

[41]S. Xu, T. Aslam, and D. S. Stewart, "High resolution numerical simulation of ideal and non-ideal compressible reacting flows with embedded internal boundaries," Combustion Theory and Modelling **1**, 113–142 (1997).

[42]A. Mignone, P. Tzeferacos, and G. Bodo, "High-order conservative finite difference GLM–MHD schemes for cell-centered MHD," Journal of Computational Physics **229**, 5896–5920 (2010).

[43]E. F. Toro, M. Spruce, and W. Speares, "Restoration of the contact surface in the HLL-riemann solver," Shock waves **4**, 25–34 (1994).

[44]G. Taylor, "The dynamics of the combustion products behind plane and spherical detonation fronts in explosives," Proceedings of the Royal Society of London A: Mathematical, Physical and Engineering Sciences **200**, 235–247 (1950).

[45]A. Sow, *Modélisation numérique des détonations gazeuses en milieu confiné*, Ph.D. thesis, University of Rouen (2014).

[46]J. J. Erpenbeck, "Stability of idealized one-reaction detonations," Physics of Fluids **7**, 684–696 (1964).

[47]W. Fickett and W. W. Wood, "Flow calculations for pulsating one-dimensional detonations," Physics of Fluids **9**, 903–916 (1966).

[48]H. D. Ng and F. Zhang, in *Shock Waves Science and Technology Library, Vol. 6* (Springer, 2012) pp. 107–212.

[49]H. D. Ng, A. J. Higgins, C. B. Kiyanda, M. I. Radulescu, J. H. S. Lee, K. Bates, and N. Nikiforakis, "Nonlinear dynamics and chaos analysis of one-dimensional pulsating detonations," Combustion Theory and Modelling **9**, 159–170 (2005).

[50]R. Klein and D. S. Stewart, "The relation between curvature, rate state-dependence, and detonation velocity," SIAM Journal on Applied Mathematics **53**, 1401–1435 (1993).

[51]S. Tsuge, H. Furukawa, M. Matsukawa, and T. Nakagawa, "On the dual property and the limit of hydrogen-oxygen free detonation waves," Astronaut. Acta **15**, 377–386 (1970).

[52]A. Savitzky and M. J. E. Golay, "Smoothing and differentiation of data by simplified least squares procedures." Analytical Chemistry **36**, 1627–1639 (1964).

[53]A. Sow, A. Chinnayya, and A. Hadjadj, "Computational study of non-ideal and mildly-unstable detonation waves," Computers & Fluids **119**, 47 – 57 (2015).

[54]A. Higgins, "Steady one-dimensional detonations," in *Shock Waves Science and Technology Library, Vol. 6* (Springer, 2012) pp. 33–105.

[55]J.-P. Dionne, H. D. Ng, and J. H. S. Lee, "Transient development of friction-induced low-velocity detonations," Proceedings of the Combustion Institute **28**, 645 – 651 (2000).

[56]S. D. Watt and G. J. Sharpe, "One-dimensional linear stability of curved detonations," Proceedings of the Royal Society of London A: Mathematical, Physical and Engineering Sciences **460**, 2551–2568 (2004).

[57]A. Sow, A. Chinnayya, and A. Hadjadj, "Mean structure of one-dimensional unstable detonations with friction," Journal of Fluid Mechanics **743**, 503–533 (2014).

[58]B. Borzou and M. I. Radulescu, "Dynamics of detonations with a constant mean flow divergence," arXiv preprint arXiv:1606.05323 (2016).

[59]F. Pintgen, C. A. Eckett, J. M. Austin, and J. E. Shepherd, "Direct observations of reaction zone structure in propagating detonations," Combustion and Flame **133**, 211 – 229 (2003).

[60]K. Mazaheri, Y. Mahmoudi, M. Sabzpooshani, and M. I. Radulescu, "Experimental and numerical investigation of propagation mechanism of gaseous detonations in channels with porous walls," Combustion and Flame **162**, 2638 – 2659 (2015).

[61]A. Favre, "Equations des gaz turbulents compressibles," Journal de mecanique **4**, 361–390 (1965).

[62]M. I. Radulescu, G. J. Sharpe, C. K. Law, and J. H. S. Lee, "The hydrodynamic structure of unstable cellular detonations," Journal of Fluid Mechanics **580**, 31–81 (2007).

[63]R. I. Soloukhin, "Nonstationary phenomena in gaseous detonation," Symposium (International) on Combustion **12**, 799 – 807 (1969).

[64]J. H. S. Lee and M. I. Radulescu, "On the hydrodynamic thickness of cellular detonations," Combustion, Explosion and Shock Waves **41**, 745–765.

[65]A. A. Vasil'ev, T. P. Gavrilenko, and M. E. Topchian, "On the Chapman-Jouguet surface in multi-headed gaseous detonations," **17**, 499–502 (1972).

[66]D. H. Edwards, A. T. Jones, and D. E. Phillips, "The location of the chapman-jouguet surface in a multiheaded detonation wave," Journal of Physics D: Applied Physics **9**, 1331 (1976).

[67]I. O. Moen, A. Sulmistras, G. O. Thomas, D. Bjerketvedt, and P. A. Thibault, "Influence of cellular regularity on the behavior of gaseous detonations," Progress in Astronautics and Aeronautics **106**, 220–243 (1986).

[68]S. Laberge, R. Knystautas, and J. H. S. Lee, "Propagation and extinction of detonation waves in tube bundles," Progress in Astronautics and Aeronautics **153**, 381–381 (1993).

[69]A. Camargo, H. D. Ng, J. Chao, and J. H. S. Lee, "Propagation of near-limit gaseous detonations in small diameter tubes," Shock Waves **20**, 499–508 (2010).

[70]Y. Gao, B. Zhang, H. D. Ng, and J. H. S. Lee, "An experimental investigation of detonation limits in hydrogen–oxygen–argon mixtures," International Journal of Hydrogen Energy **41**, 6076 – 6083 (2016).

[71]M. Weber and H. Olivier, "The thickness of detonation waves visualised by slight obstacles," Shock Waves **13**, 351–365 (2003).

[72]G. Jarsalé, F. Virot, and A. Chinnayya, "Ethylene–air detonation in water spray," Shock Waves (2016).

[73]J. B. Bdzil and D. S. Stewart, "Time-dependent two-dimensional detonation: the interaction of edge rarefactions with finite-length reaction zones," Journal of Fluid Mechanics **171**, 1–26 (1986).

[74]S. Murray and J. Lee, "The influence of physical boundaries on gaseous detonation waves," Prog. Astronaut. Aeronaut **106**, 329–355 (1986).

[75]K. Y. Cho, J. R. Codoni, B. A. Rankin, J. Hoke, and F. Schauer, "Effects of lateral relief of detonation in a thin channel," in *55th AIAA Aerospace Sciences Meeting* (2017) p. 0373.

[76]A. A. Vasil'ev, "Critical diameter of gas-mixture detonation," Combustion, Explosion and Shock Waves **18**, 349–355 (1982).

[77]R. Fievisohn and K. Yu, "Method of characteristic analysis of gaseous detonations bounded by an inert gas," (2015).

[78]A. Borisov, S. Khomic, and V. Mikhalkin, "Detonation of unconfined and semiconfined charges of gaseous mixtures," Prog. Astronaut. Aeronaut **133**, 118–132 (1991).

[79]L. M. Faria and A. R. Kasimov, "Qualitative modeling of the dynamics of detonations with losses," Proceedings of the Combustion Institute **35** (2015).

[80]C. B. Kiyanda and A. J. Higgins, "Photographic investigation into the mechanism of combustion in irregular detonation waves," Shock Waves **23**, 115–130 (2013).

[81]J. H. S. Lee, "The universal role of turbulence in the propagation of strong shocks and detonation waves," in *High-Pressure Shock Compression of Solids VI: Old Paradigms and New Challenges*, edited by Y. Horie, L. Davison, and N. N. Thadhani (Springer New York, New York, NY, 2003) pp. 121–148.

[82]V. A. Subbotin, "Collision of transverse detonation waves in gases," Combustion, Explosion and Shock Waves **11**, 411–414.

[83]J. M. Austin, F. Pintgen, and J. E. Shepherd, "Reaction zones in highly unstable detonations," Proceedings of the Combustion Institute **30**, 1849 – 1857 (2005).

[84]M. I. Radulescu, G. J. Sharpe, J. H. S. Lee, C. B. Kiyanda, A. J. Higgins, and R. K. Hanson, "The ignition mechanism in irregular structure gaseous detonations," Proceedings of the Combustion Institute **30**, 1859 – 1867 (2005).

[85]L. Massa, J. M. Austin, and T. L. Jackson, "Triple-point shear layers in gaseous detonation waves," Journal of Fluid Mechanics **586**, 205 (2007).

[86]K. Mazaheri, Y. Mahmoudi, and M. I. Radulescu, "Diffusion and hydrodynamic instabilities in gaseous detonations," Combustion and Flame **159**, 2138 – 2154 (2012).

[87]Y. Mahmoudi and K. Mazaheri, "High resolution numerical simulation of triple point collision and origin of unburned gas pockets in turbulent detonations," Acta Astronautica **115**, 40 – 51 (2015).

[88]Y. Mahmoudi, N. Karimi, R. Deiterding, and S. Emami, "Hydrodynamic instabilities in gaseous detonations: comparison of Euler, Navier–Stokes, and large-eddy simulation,"

Journal of Propulsion and Power **30**, 384–396 (2014).